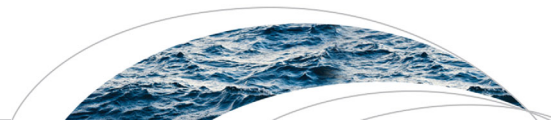


Predicting glacio-hydrologic change in the headwaters of the Zongo River, Cordillera Real, Bolivia

The Faculty of Oregon State University has made this article openly available.
Please share how this access benefits you. Your story matters.

Citation	Frans, C., Istanbuloglu, E., Lettenmaier, D. P., Naz, B. S., Clarke, G. K., Condom, T., ... & Nolin, A. W. (2015). Predicting glacio-hydrologic change in the headwaters of the Zongo River, Cordillera Real, Bolivia. <i>Water Resources Research</i> , 51(11), 9029-9052. doi:10.1002/2014WR016728
DOI	10.1002/2014WR016728
Publisher	John Wiley & Sons, Inc.
Version	Version of Record
Terms of Use	http://cdss.library.oregonstate.edu/sa-termsfuse



RESEARCH ARTICLE

10.1002/2014WR016728

Predicting glacio-hydrologic change in the headwaters of the Zongo River, Cordillera Real, Bolivia

Chris Frans¹, Erkan Istanbuluoglu¹, Dennis P. Lettenmaier², Bibi S. Naz³, Garry K. C. Clarke⁴, Thomas Condom⁵, Pat Burns^{6,7}, and Anne W. Nolin⁶

Key Points:

- Representation ice flow is critical to depict phased hydrologic response to glacier recession
- Predictions of glacier and runoff patterns are highly sensitive to the selection of energy balance parameters
- Increased evapotranspiration is critical to consider in long-term projections of water availability

Supporting Information:

- Supporting Information S1

Correspondence to:

C. Frans,
chrisf2@uw.edu

Citation:

Frans, C., E. Istanbuluoglu, D. P. Lettenmaier, B. Naz, G. Clarke, T. Condom, P. Burns, and A. Nolin (2015), Predicting glacio-hydrologic change in the headwaters of the Zongo River, Cordillera Real, Bolivia, *Water Resour. Res.*, 51, 9029–9052, doi:10.1002/2014WR016728.

Received 24 NOV 2014

Accepted 20 OCT 2015

Accepted article online 29 OCT 2015

Published online 19 NOV 2015

¹Department of Civil and Environmental Engineering, University of Washington, Seattle, Washington, USA, ²Department of Geography, University of California, Los Angeles, California, USA, ³Oak Ridge National Laboratory, Oak Ridge, Tennessee, USA, ⁴Department of Earth, Ocean, and Atmospheric Sciences, University of British Columbia, Vancouver, British Columbia, Canada, ⁵IRD, Univ. Grenoble Alpes, CNRS, G-INP, LTHE (UMR 5564), Grenoble, France, ⁶College of Earth, Ocean, and Atmospheric Sciences, Oregon State University, Corvallis, Oregon, USA, ⁷Now at Quantum Spatial, Portland, Oregon, USA

Abstract In many partially glacierized watersheds glacier recession driven by a warming climate could lead to complex patterns of streamflow response over time, often marked with rapid increases followed by sharp declines, depending on initial glacier ice cover and rate of climate change. Capturing such “phases” of hydrologic response is critical in regions where communities rely on glacier meltwater, particularly during low flows. In this paper, we investigate glacio-hydrologic response in the headwaters of the Zongo River, Bolivia, under climate change using a distributed glacio-hydrological model over the period of 1987–2100. Model predictions are evaluated through comparisons with satellite-derived glacier extent estimates, glacier surface velocity, in situ glacier mass balance, surface energy flux, and stream discharge measurements. Historically (1987–2010) modeled glacier melt accounts for 27% of annual runoff, and 61% of dry season (JJA) runoff on average. During this period the relative glacier cover was observed to decline from 35 to 21% of the watershed. In the future, annual and dry season discharge is projected to decrease by 4% and 27% by midcentury and 25% and 57% by the end of the century, respectively, following the loss of 81% of the ice in the watershed. Modeled runoff patterns evolve through the interplay of positive and negative trends in glacier melt and increased evapotranspiration as the climate warms. Sensitivity analyses demonstrate that the selection of model surface energy balance parameters greatly influences the trajectory of hydrological change projected during the first half of the 21st century. These model results underscore the importance of coupled glacio-hydrology modeling.

1. Introduction

Recession of alpine glaciers has been observed across much of the globe in recent decades [Kaser *et al.*, 2006; Gardner *et al.*, 2013; IPCC, 2014]. Glacier recession is projected to continue throughout the 21st century in response to continued climate warming [Radić and Hock, 2011] resulting in decreased seasonal water storage for many populated areas located downstream from these dynamic cryospheric systems [Barnett *et al.*, 2005]. Some of the largest decreases in glacier mass have been observed in the tropical glaciers of the South American Andes, which have been receding rapidly (-0.76 m w.e. yr^{-1}) since the late 1970s in response to increasing air temperature [Rabatel *et al.*, 2013].

Predictions from Global Climate Models (GCMs) indicate that the observed warming will continue, and will be amplified at higher altitudes in the lower troposphere in the Andean cordilleras of Ecuador, Peru, Bolivia and Northern Chile [Bradley *et al.*, 2006]. The glaciers of the tropical Andes are closely linked to the water resources of the region due to their proximity to highly populated areas and the ability of glacier melt water to buffer highly seasonal precipitation patterns [Vuille *et al.*, 2008]. Meltwater from the glaciers in the Andes plays an important role in socio-economic infrastructure of the region. It provides municipal and industrial water supply, irrigation water, hydropower, and supports ecosystem services [Mark and Seltzer, 2003; Vergara *et al.*, 2007; Chevallier *et al.*, 2011; Cauvy-Fraunié *et al.*, 2013].

Glacier melt is manifested by a unique signature in catchment runoff response. The melting of snow and ice modulates seasonal availability of water by redistributing wet season precipitation into runoff during the

dry season. In contrast to seasonal snow, glaciers often produce anomalously large runoff during dry and warm years [Fountain and Tangborn, 1985]. For this reason, as the climate warms, runoff is expected to increase initially as a result of increased rates of ablation per unit area (typically for several decades, depending on the particulars of the glacier and climate), however the glacier's area will eventually reduce to a point where runoff will decline thereafter [e.g., Huss et al., 2008; Lambrecht and Mayer, 2009; Moore et al., 2009; Baraer et al., 2012].

Understanding the distinct phases of the response of partially glacierized watersheds to glacier ice loss, and estimating the current phases of transitioning watersheds remains an important challenge in regions where glacial melt supplies anthropogenic and ecologic systems downstream. Glaciological methods, including field measurements, remote sensing and modeling, have been applied to describe the relative role of glaciers in these changing systems [La Freniere and Mark, 2014]. Previous studies analyzing the contribution of glaciers to water resources in the Andes have utilized multitemporal estimates of glacier area and volume derived from satellite and aerial imagery [e.g., Soruco et al., 2009; Burns and Nolin, 2014] that describe glacier change relative to total watershed drainage area. Remote sensing can be an effective tool for monitoring glacier change over annual [e.g., Rabatel et al., 2012] or decadal [e.g., Soruco et al., 2009] timescales, although used in isolation, it reveals little about the relative and changing contributions of glacier melt to watershed hydrology because it provides only estimates of glacier spatial extent and volume. These estimates reflect changes at coarse temporal scales and do not account for the interaction and the relative role of melt water with the nonglacierized watershed between the glaciers and downstream locations. Alternatively, statistical trend analyses of time series of discharge for individual watersheds have been applied to identify trends and phases of hydrologic response to glacier recession [e.g., Baraer et al., 2012; Stahl and Moore, 2006; Casassa et al., 2009]. However, many partially glacierized watersheds lack observations of discharge of suitable length, which is detrimental, because glacier recession and its hydrologic response often occur over long periods of time. Moreover, time series of discharge observations alone do not allow identification of the mechanisms that control changing inter-annual and decadal variations in discharge from transitional partially glacierized river basins.

Efforts have been made to model the coupled glacio-hydrologic behavior of partially glacierized high Andes watersheds using relatively simple hydrologic models that use spatially "lumped" and empirical representations of watershed processes [e.g., Pouyaud et al., 2005; Juen et al., 2007; Suarez et al., 2008; Baraer et al., 2012; Condom et al., 2012; Chevallier et al., 2011; Soruco et al., 2015]. Some modeling studies have used volume-area scaling relationships to simulate changes in glacier extent with changes in glacier mass [Baraer et al., 2012; Condom et al., 2012]. However, the accuracy of this method is debated because scaling parameters evolve over time under transient glacier change [Radić et al., 2007; Adhikari and Marshall, 2012], vary spatially [Huss and Farinotti, 2012], and do not represent characteristics of individual glaciers (e.g., local topographic controls on surface geometry). Most glacio-hydrologic studies in the Andes have not explicitly considered the role of glacier dynamic ice flow in the simulation of glacier area. While neglecting the influences of glacier dynamics on glacier area may be justifiable for near term predictions of glacier runoff production, it is essential for accurately predicting the effects of evolving glacier area over long periods of time for the prediction of watershed hydrology [Huss et al., 2008; Immerzeel et al., 2012; Naz et al., 2014; Uhlmann et al., 2012a, 2012b].

Understanding and predicting the multifaceted nature of glacier response (area, volume, discharge) and its coupling with watershed hydrology under climate variability and change is crucial in regions with rapidly melting glaciers. In this paper we present a comprehensive approach to investigate implications of climate change on glacierized watersheds by integrating glaciological field observations, remote sensing observations of changing glacier extent, and distributed glacio-hydrological modeling guided and constrained by these observations. We use our approach to infer long term hydrologic change in the headwaters of the Zongo River located near La Paz, Bolivia in the South American Andes. The main objectives of this study are (1) to investigate and quantify the glacio-hydrologic response to historic climatic conditions in a watershed where glacier melt has had a strong influence on discharge; (2) to evaluate and predict how this glacio-hydrologic system will change under future climate conditions; and (3) demonstrate the influence of parameter selection and calibration on model projections using an advanced glacio-hydrology simulation model.

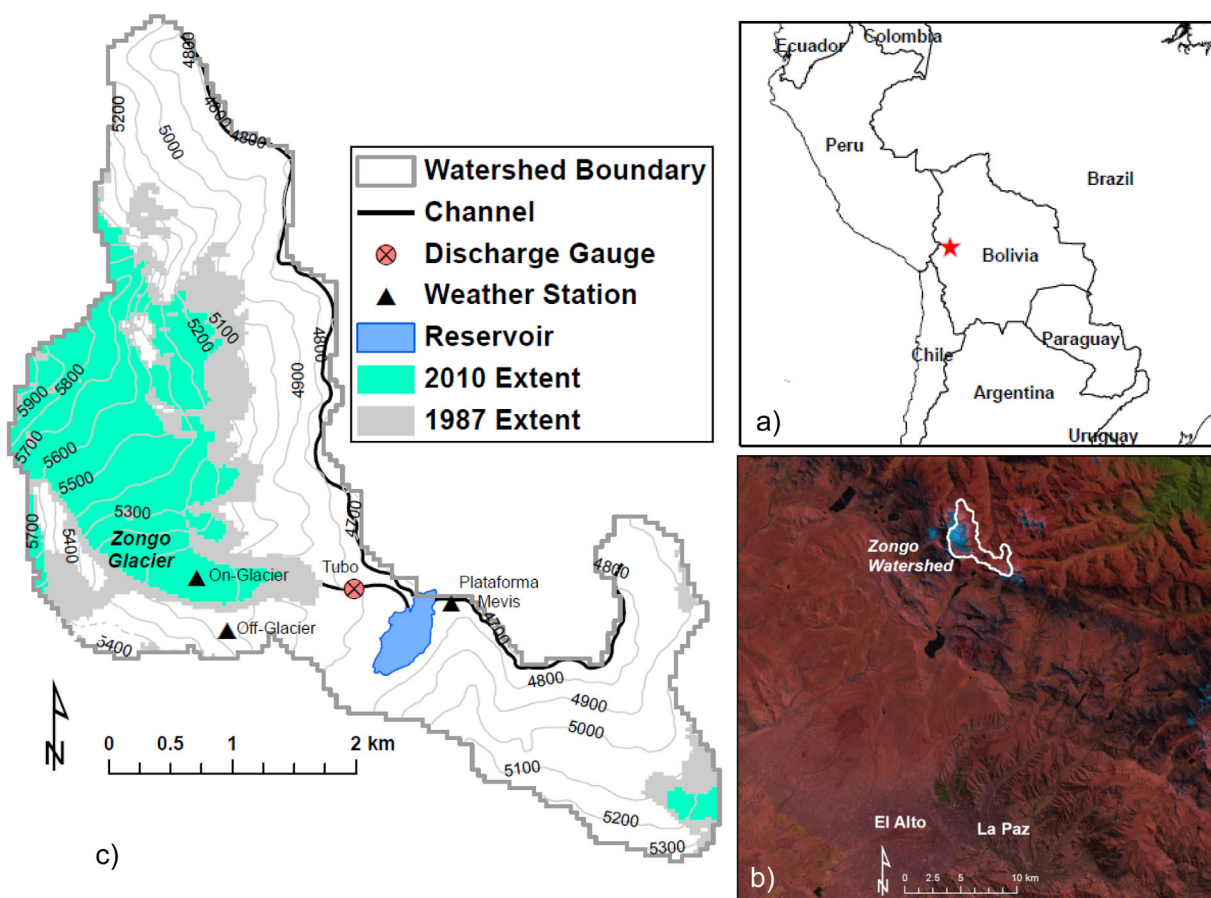


Figure 1. Zongo headwaters study site in Bolivia: (a) regional map, red star indicates the location of the study site; (b) false color satellite image including La Paz and El Alto; (c) watershed map showing equal elevation lines (m), glacier historical extent from Landsat-TM imagery, and in situ observation locations.

2. Study Site

The headwaters of the Zongo River (16 °S, 68 °W) are located in the Cordillera Real, 30 km north of La Paz (the capital city of Bolivia) and El Alto, a large and rapidly expanding urban area (Figure 1). The 14 km² drainage area is defined by the crest of the Cordillera Real along the southwestern perimeter of the catchment (which divides the Altiplano to the west from Amazon basin to the east) and manmade conveyance channels on the northeastern slopes that divert runoff to a reservoir located near the middle of the catchment (Figure 1). The study domain includes the entire drainage area above the Zongo Reservoir. This extends the domain beyond previous hydrological studies in the area that focused modeling and observational analyses on the 3 km² drainage area above the Tubo discharge measurement location (Figure 1) below the terminus of Zongo glacier [e.g., Ribstein *et al.*, 1995; Francou *et al.*, 1995; Wagon *et al.*, 1999; Sicart *et al.*, 2011]. Elevations within the basin range from 4700 to 6088 m a.s.l. at the summit of Huayna Potosi. In the watershed glacier cover decreased from 35% in 1987 to 21% in 2010 (estimates derived from Landsat imagery, section 4.4). The catchment is characterized by bare rock and thin soils. Where vegetation is present, it consists of sparse grasses (25%) and shrubs (17%). The catchment is the upper reach of a hydroelectric project consisting of 10 downstream power generation facilities in series along the Zongo River. These facilities have a total capacity of 174.6 MW, and provide much of the electricity for the La Paz area [Caballero *et al.*, 2004]. Runoff is stored in the reservoir (Figure 1) and is released during the dry season.

The watershed is located in the outer tropics, with a climate characterized by distinct seasonal variability in atmospheric moisture. Documenting this climate, precipitation and temperature have been measured at the Plataforma and Mevis station locations (Figure 1), respectively, for an extended period of time. During austral summer, November to March, wet and relatively warm (2.5°C on average, calculated from half-hourly

observations at the Mevis station, 4750 m, 1995–2010) conditions prevail while dry and slightly cooler (1.2°C on average) periods persist during austral winter, June to September. The seasonal variation of daily average temperature is relatively small ($<8^{\circ}\text{C}$) [Sicart *et al.*, 2011] while precipitation and atmospheric moisture follow a strong seasonal pattern. Mean annual precipitation observed at the Plataforma observation location (4750 m) for the 1971–2003 period is 805 mm, 77% of which occurred between November and March.

Frequent cloud cover during the wet season, when the extraterrestrial solar radiation flux is at its maximum, attenuates the seasonal variability in shortwave radiation at the land surface in this region. Nonetheless, clear conditions during the wet season (summer) at this latitude (high sun elevation) and altitude (low optical depth) of the study site lead to very high downward shortwave radiation (mean daily values in the wet season are $\sim 80\text{ W m}^{-2}$ less than extraterrestrial irradiance according to Sicart *et al.* [2005]). Downward longwave radiation follows the seasonality of humidity and cloud cover, with a maximum during the wet season and minimum during the dry season. Clear sky emissivity is low at this high altitude, which promotes net losses of longwave radiation at the surface of snow and ice, providing significant control over surface energy dynamics during the dry season [Sicart *et al.*, 2005].

During the wet season, precipitation is largely associated with advection of moist air from the eastern interior continent linked with the South American monsoon [Garreaud *et al.*, 2009]. Wet season precipitation varies inter-annually with sea surface temperature (SST) of the equatorial Pacific Ocean. At times of high sea surface temperatures offshore (El Niño), advection of moisture from the east is suppressed through increased westerly atmospheric flow, leading to below average wet season precipitation [Vuille *et al.*, 2000]. During El Niño anomalies, glacier mass balance is most frequently negative, as precipitation in the form of snow largely controls not only the mass, but the energy budget of the glaciers as fresh snow increases the reflection of incoming solar radiation [Sicart *et al.*, 2011]. During La Niña years the glacier mass balance is typically near equilibrium or slightly positive [Francou *et al.*, 2003]. Glacier ablation occurs throughout the year. Peak glacier ablation occurs during the transitional period leading into the wet season in the austral summer, after which fresh snowfall covers a large fraction of the glacier surface. During the wet season watershed discharge is dominated by rainfall, transient snow melt [Lejeune *et al.*, 2007], and to a lesser extent, glacier melt at the lowest elevations on the glaciers. Glacier ablation is most critical to discharge during the dry season when precipitation reaches a minimum [e.g., Ribstein *et al.*, 1995; Wagnon *et al.*, 1999; Sicart *et al.*, 2011].

3. Approach

3.1. Glacio-Hydrological Model

To simulate the glacial and hydrologic processes across the watershed we used the Distributed Hydrology Soil Vegetation Model (DHSVM) [Wigmosta *et al.*, 1994], coupled with a glacier dynamics model [Clarke *et al.*, 2015] as described by Naz *et al.* [2014]. A brief description of the components of the models and their coupling is provided herein, with model components and linkages shown in Figure 2. For a complete description of the model, the reader is referred to Naz *et al.* [2014]. DHSVM is a fully distributed physically based hydrology model. It has been widely applied in the mountainous Western United States [e.g., Storck *et al.*, 1998; Elsner *et al.*, 2010; Cristea *et al.*, 2013] as well as other regions throughout the world [e.g., Cuo *et al.*, 2006; Zhao *et al.*, 2009]. The surface energy balance (SEB) snow model in DHSVM consists of two snow layers [Andreadis *et al.*, 2009]. In grid cells where glaciers exist (determined by the prescribed initial condition, advancing flow of ice, or snow densification to ice) a layer representing glacier ice is included below the lower snow layer. Melting of the surface of the glacier ice layer is simulated when the snow layers have melted completely, and excess energy is available for melt as calculated through the SEB algorithms. Snow accumulation and ablation in nonglacierized grid cells is simulated using the 2 layer SEB model.

The simulation of surface accumulation and ablation processes described above is coupled with the simulation of dynamic flow of glacier ice. Glacier surface mass balance is modeled at hourly time steps through snow accumulation and ablation, glacier ice ablation, and snow densification to ice. At the end of each month, the net change in the mass of the ice as a result of vertical fluxes of accumulation and ablation is calculated at every glacierized grid cell to develop a “mass balance” field (b : meters water equivalent, m w.e.), used to force the glacier dynamics submodel of DHSVM. Dynamic cell to cell ice flow is then simulated based on a vertically integrated shallow ice approximation of the continuum mechanics equations

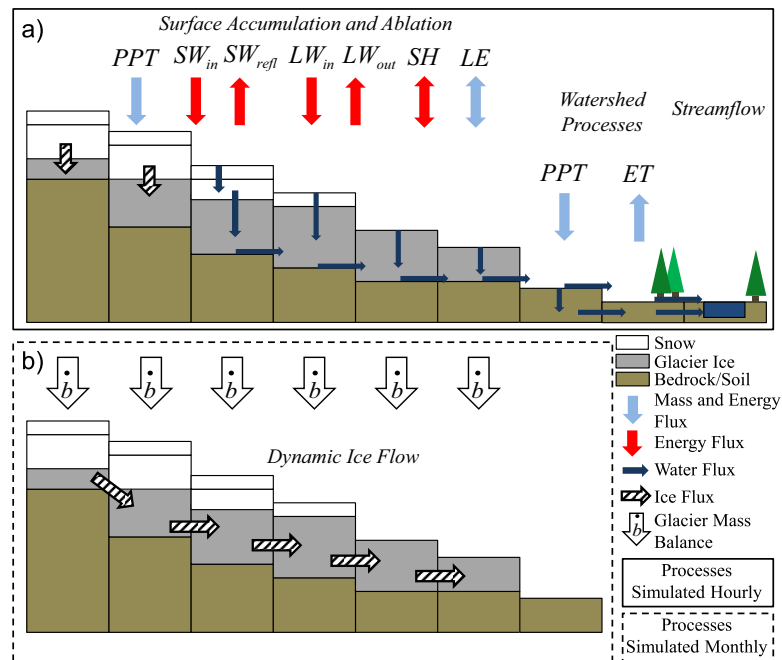


Figure 2. Schematic showing the first order processes simulated by the coupled glacier-hydrology model. (a) Land surface and hydrology component of the coupled model illustrating the fluxes of mass and energy between the atmosphere and land surface implemented on snow, glacier ice, and soil/vegetation surfaces. Arrows indicate precipitation, PPT ; incoming shortwave radiation, SW_{in} ; reflected shortwave radiation, SW_{refl} ; downwelling longwave radiation, LW_{in} ; emitted longwave radiation, LW_{out} ; sensible heat, SH ; latent heat, LE ; and evapotranspiration, ET . (b) Illustration of the glacier dynamics component of the model that simulates lateral dynamic ice flow driven by gravity as ice accumulates with positive ice mass balance (b).

governing ice deformation and sliding [e.g., Mahaffy, 1976; Plummer and Phillips, 2003] as formulated in Clarke et al. [2015] as a diffusion equation:

$$\frac{\partial S}{\partial t} = \nabla_{xy} \cdot (D \nabla_{xy} S) + \frac{\rho_{ice} \dot{b}}{\rho_w} \quad (1)$$

The change in surface elevation from the flow of ice (∂S) is driven by ice surface slope ($\nabla_{xy} S$), momentum diffusivity (D), and \dot{b} simulated over the preceding month. Diffusivity is a nonlinear function of ice thickness (H) and surface slope ($\nabla_{xy} S$):

$$D(H, S_{xy}) = \frac{2A(\rho_{ice}g)^n |\nabla_{xy} S|^{n-1}}{n+2} H^{n+2} + C(\rho_{ice}g)^m |\nabla_{S_{x,y}}|^{m-1} H^m \quad (2)$$

The first term of (2) represents Glen’s flow law for ice creep, with parameters $A = 7.5738 \times 10^{-17} \text{ Pa}^{-3} \text{ yr}^{-1}$ and $n=3$ [Glen, 1955]. The second term of (2) represents basal sliding with $m = 3$, the sliding law exponent, and C being the sliding law coefficient. It is likely that basal sliding contributes to ice movement to some extent. However given the uncertainties in selecting a value for the C parameter for all glaciers in the domain, in this study basal sliding was not modeled (i.e., $C=0$). Arguably, for shrinking glaciers the processes that drive the sliding component of flow are likely to diminish over time [Clarke et al., 2015]. However, in section 5.4 we do provide a sensitivity analysis of model results using a model configuration that includes basal sliding. Accounting for simulated ice flow through creep, the thickness and extent of glacier ice layers are updated at a monthly time step, while the SEB and distributed watershed hydrologic processes (e.g., evapotranspiration, surface/subsurface flow, channel routing, snow accumulation and ablation, etc.) are continuously simulated at an hourly simulation time step.

3.2. Initializing Glacier Extent and Thickness

Uncertainties in the extent and thicknesses of glacier ice used in glacio-hydrologic model applications could lead to highly uncertain model projections of hydrologic change and runoff in a warming climate [Huss

Table 1. Range of Parameters Sampled and Optimal Parameter Values Used in Simulations

Model Parameter	Range Analyzed	Optimal
Snow Roughness Length (mm)	0.5–5	0.7
Precipitation Elevation Gradient (%/km)	0–100	15
Temperature Lapse Rate (°C/m)	–0.009 to –0.003	–0.0084
Maximum Snow Albedo	0.8–0.9	0.83
Glacier Ice Albedo	0.3–0.4	0.39

et al., 2014]. To accurately estimate the glacier extent and distribution of ice thickness at the beginning of the historical simulation period we used a four step spin-up procedure. In step 1, we calculated a mean annual surface mass balance field (\bar{b}) that is spatially distributed across the model domain to use as model forcing. This field was computed by running the hourly SEB snow/ice model of DHSVM from 1987 to 2010 using meteorological data described in section 4.2.

Hourly fluxes were summed to estimate net annual change of glacier mass in each modeled year. Taking the mean of annual estimates, a mean annual net change of the ice layer (\bar{b}) at each grid cell is calculated. Glacier ice was assumed to always be available to melt at every grid cell location when no snow was present so that the mass balance field was spatially continuous throughout the model domain. In step 2, the glacier dynamics model was run offline (decoupled from the hydrology model) with no initial glacier thickness on the landscape, driven with constant \bar{b} until a steady-state glacier ice distribution is reached. Forcing the glacier dynamics model with \bar{b} calculated from recent meteorological data produces steady state ice masses that are much smaller than are observed in historical extent estimates because the ice masses present in recent decades are largely the result of past colder climate conditions. In step 3, we perturbed the mass balance forcing (\bar{b}) calculated in step 1 so that the extent of modeled steady state ice masses closely matches the earliest historical ice extent estimate. Up to 0.85 m w.e. was added to \bar{b} to obtain a match with the observed estimate. Glacier extent derived from a 1987 Landsat image is taken as the earliest ice extent estimate. Large ice masses (Zongo Glacier) required the largest perturbation while small high elevation masses required small or no perturbation in equilibrium mass balance.

Following step 3, we obtained mechanically stable ice masses that closely matched historical glacier area estimates. However, these ice masses reflect a steady state condition, which is unrealistic for the actual state of the glaciers of this region in the mid-1980s [Rabatel *et al.*, 2013]. To represent a thinner, more realistic transient distribution of ice mass with which to initialize the hydrology model for historical simulations, a fourth step in the spin-up process was required. Accordingly, in step 4 we ran the full SEB model with the steady state ice masses from step 3, that match the boundaries of the earliest ice extent, with the hourly historical meteorological forcing data for 5 years to thin the glacier thicknesses to a representative transient state. We used an iterative procedure to determine the number of years to use in this “thinning” simulation. We found 5 years as a sufficiently long duration for the thinning run, after which the model consistently predicted glacier recession, glacier discharge and streamflow (e.g., Figure 5, see section 5.1).

3.3. Model Calibration and Evaluation

We calibrated the model using a multiobjective complex evolution global optimization method (MOCOM-UA) [Yapo *et al.*, 1998] over the historical time period where observational data are available in space and time. In model calibration, our objective was to maximize the Nash-Sutcliffe Efficiency (NSE) calculated for streamflow and log transformed streamflow, and minimize the root mean square error (RMSE) of annual net mass balance of the Zongo glacier to find optimal parameter values in calibration. To provide ranges for realistic calibration parameters, we conducted initial trial and error parameter sensitivity analyses using parameter values in published literature. Through calibration we identified critical, spatially uniform, model parameters that improve model predictions. Parameters adjusted during model calibration included temperature lapse rate, precipitation lapse rate, maximum snow albedo, aerodynamic roughness length over snow, and glacier ice albedo. Precipitation and temperature lapse rates, snow albedo, and glacier albedo have been measured at a limited number of locations in the study area. However directly using field-estimated local parameter values did not consistently improve model predictions with respect to streamflow and glacier spatial and temporal evolution. Therefore to capture representative parameter values at the watershed-scale, sampling parameters from their physically realistic ranges as guided by field observations and literature values deemed appropriate in this study. This approach would also partially compensate for any biases in the forcing data. The ranges of the parameter values evaluated and the optimal values obtained from model calibration are listed in Table 1.

4. Data

4.1. Geospatial Data

Our modeling approach requires spatial characterization of elevation, soil depth and texture, vegetation, meteorological forcing, and the initial distribution of glacier ice described in section 3.2. We applied DHSVM at a grid resolution of 50 m. Digital elevation model (DEM) data were acquired from the Advanced Spaceborne Thermal Emission and Reflection Radiometer (ASTER) Global Digital Elevation Model Version 2 (GDEM V2) elevation product (NASA-USA, METI-Japan). In areas where artificial canals cross the watershed (Figure 1) the DEM elevations were modified by decreasing elevations in the canals so that surface runoff is intercepted and conveyed to the reservoir. We estimated glacier bed topography (the elevation of the land surface under the glaciers) by running a bed stress model that calculates basal shear stress as a linear optimization problem and uses a DEM (surface topography including current glacier ice), modeled mass balance fields, and observed ice thinning rates as model input [Clarke *et al.*, 2013].

We estimated soil depths across the basin empirically from topography, based on elevation, local slope and contributing area [Westrick, 1999]. This algorithm gives thin soils on steep slopes and ridge tops and thicker soils on gentle slopes and in depressions, within a defined range of 0.2 – 4.25 m based largely on conjecture. Soil classification data available for remote areas (e.g., Harmonized World Soil Database) are often of a spatial resolution that is too coarse for watershed scale hydrological modeling. Hence, soil texture classes were also estimated based on local slope and contributing area, with finer soils (fluvial-glacial deposits) specified in areas of low relief and high contributing areas and coarser soils (talus, lateral moraines) and bedrock specified where slopes are steep. The soil type under glaciers was specified as bedrock. This slope-derived distribution of soil texture is consistent with those described and mapped in Caballero *et al.* [2002] at a coarser spatial representation of a larger area. Vegetation was specified following an inventory of digital land cover data (Centro Digital de Recursos Naturales de Bolivia, CDRNB, <http://essm.tamu.edu/bolivia/>), and manually adjusted where it was not consistent with Google Earth imagery.

4.2. Historical Meteorological Data

The historical period we selected for model calibration and analysis is 1987–2010, based on the availability of high quality satellite imagery suitable for glacier area delineation. DHSVM's required meteorological forcings include surface air temperature, relative humidity, wind speed, downward shortwave and longwave radiation, and precipitation. An hourly model time step was preferred to account for the high diurnal variability in the surface energy dynamics. The Institute of Research for Development (IRD, France, GLACIOCLIM GREATICE projects) and Compañía Boliviana de Energía Eléctrica (COBEE, a private hydroelectric utility company) have maintained intermittent and ongoing meteorological measurement stations in the basin for several decades. However, continuous hourly measurements of all of the required input variables with limited periods of missing data are only publicly available from hydrological year 2004–2009 at the Off-Glacier station (Figure 1) (<http://www-lgge.ujf-grenoble.fr/ServiceObs/>). This limited period is not sufficient for historical model calibration, validation, and analysis of hydrological change.

In order to run the model for the historical period, a longer hourly time series of meteorological forcing data was generated through bias correction of reanalysis meteorological data, Modern Era Retrospective-Analysis for Research and Applications (MERRA, NASA). MERRA data are available from 1979 through present. We removed systematic biases from the MERRA reanalysis products using the available observed data at the Off-Glacier station and the methods described in Berg *et al.* [2003], which were extended to finer time scales to account for diurnal biases. Raw MERRA data had large biases in magnitudes and did not realistically capture diurnal patterns when compared to the observations at the Off-Glacier station. This is largely due to the coarse spatial resolution ($1/2 \times 2/3^\circ$) of the MERRA output. Therefore to remove systematic diurnal and seasonal biases in the reanalysis data, we used the observed station and reanalysis data for 2004–2009 (dates with missing data removed from both sources), and computed ratios for shortwave radiation, relative humidity, wind speed, as well as absolute differences in air temperature, using the monthly mean of each hour of the day for each month of the year, and implemented corrections with the following equations. For example,

$$SW_{BC} = \frac{\overline{SW}(\text{obs})_{hr,mth}}{\overline{SW}(\text{merra})_{hr,mth}} \times SW(\text{merra}) \quad (3)$$

$$Ta_{BC} = \left(\overline{Ta}(obs)_{hr,mth} - \overline{Ta}(merra)_{hr,mth} \right) + Ta(merra) \quad (4)$$

Equation (1) gives the ratio-based bias correction (BC) of shortwave radiation (SW), whereas equation (2) gives the absolute difference bias correction of 2 m air temperature (Ta). Comparisons of the uncorrected MERRA and observational data are reported in the supporting information, section S1. Downward longwave radiation was calculated from the bias corrected relative humidity, air temperature, and shortwave radiation time series and calculated top of atmosphere solar irradiance following *Sicart et al.* [2010]. Additional stations (Figure 1) that measured single meteorological variables, Mevis (temperature) and Plataforma (precipitation) were used to evaluate raw and bias corrected meteorological data.

The MERRA surface precipitation monthly total accumulations compared well with observations at the Plataforma station (NSE = 0.69) and at the Off-Glacier location (NSE=0.76), and hence, were not adjusted for bias. Annual differences between observations and MERRA data were relatively small, 10% on average. However, as identified by *Soruco et al.* [2009] using locally observed data, precipitation undercatch is a significant problem in this catchment. Therefore, following the findings of *Soruco et al.* [2009] the MERRA precipitation was increased by 37% to account for precipitation gauge undercatch.

We confirmed the bias-corrected MERRA data against temperature observations at the Mevis station (4750 m). For this purpose we used a lapse rate of $-5.7^{\circ}\text{C km}^{-1}$, calculated by comparing the observational records at the Mevis and Off-Glacier stations, and used this to interpolate the time series to the lower elevation of the Mevis station (4750 m). The bias corrected time series of air temperature showed agreement (NSE = 0.58) with this longer record of observation (1995–2010, periods of missing observed data were removed).

The bias-corrected data are representative of a single point in the watershed, the location of the local meteorological station from which the observations were taken (Off-Glacier, Figure 1). We assumed downward longwave radiation, relative humidity, and wind speed to be spatially homogenous across the basin, while bias-corrected shortwave radiation, temperature and precipitation were estimated for each grid cell with reference to the Off-Glacier station location. To distribute temperature and precipitation across the watershed from this point we used precipitation and temperature lapse rates calibrated to obtain consistent modeled data with glacier mass and discharge observations (Table 1). Precipitation was partitioned into rain and snow using local temperature and threshold values for the maximum temperature which snowfall can occur (0.5°C) and the minimum temperature at which rainfall can occur (-0.5°C). The bias-corrected shortwave radiation data were produced relative to a horizontal surface. In DHSVM this value is distributed for each grid element to incorporate the effects of slope, aspect, and shading.

4.3. Future Meteorological Forcing Data

Projections of the future climate 2011–2100, were generated by statistically downscaling GCM outputs using the Advanced Weather Generator (AWE-GEN), of *Ivanov et al.* [2007] following methods outlined in *Fatichi et al.* [2011]. Stochastic weather generators have been successfully applied in previous coupled glacier-hydrologic modeling applications [e.g., *Stahl et al.*, 2008; *Uhlmann et al.*, 2012b; *Pellicciotti et al.*, 2014] and have the benefit of reproducing the local behavior of multiple atmospheric surface variables at subdaily time intervals. Additionally, use of the weather generator allowed us to update statistical properties through time (according to GCM predictions) and in so doing, represent a transient climate, which is required to continuously evolve the glacier ice masses. Furthermore, this approach permits the evaluation of multiple statistically plausible realizations of future meteorological forcing data rather than relying on a single deterministic projection. Based on the availability of daily projections of temperature and precipitation through the 21st century, we identified and statistically downscaled outputs from 11 GCMs (BCC-CSM1, ACCESS1, CanESM2, CCSM4, CNCRM, CSIRO-Mk3.6, GFDL-CM3, INMCM4, MIROC5, MRIGCM, NORESM1) from the CMIP5 RCP4.5 emissions pathway scenario (ensemble r1i1p1). This scenario was selected to represent moderate warming over the 21st century. The air temperature field from each GCM was taken at the 500 hPa tropospheric altitude as an index to changes at the elevation of the watershed as opposed to the 2 m air temperature which reflects a much lower altitude due to the coarse spatial resolution of the GCMs.

We outline the steps in the downscaling process here but for more detail, the reader is referred to *Fatichi et al.* [2011]. First, statistical parameters used as inputs to the weather generator were calculated from the bias corrected historical reanalysis meteorological time series at the Off-Glacier site (section 4.2). Next, the

statistical precipitation and temperature parameters for each GCM's output were calculated for historical and future time periods at the same site. These parameters include mean, variance, skewness, frequency of zero precipitation, and the coefficients of variation at multiple temporal aggregation intervals. We calculated factors of change (ratio or absolute difference between future and historical period) in the statistical parameters for each GCM. The actual values of the parameters were not directly used; only their relative changes in time with respect to their historical values were used. Next, utilizing the factors of change of all GCMs, we used the Bayesian approach of *Tebaldi et al.* [2005] to determine probability density functions (PDFs) of the factors of change for each statistical parameter. Using these PDFs, the median (most likely) factor of change for each statistical parameter was then used to change the historical weather generator parameters through time reflecting the projected future transient climate. Hence, information from the group of GCM's was integrated to calculate a single most likely factor of change for each statistical parameter that varies in time. The weather generator parameters were updated every decade to allow for the representation of inter-annual persistence in the simulation of precipitation. Updating the parameters at this coarse time interval, as opposed to annually, lead to decadal step changes in the future meteorological time series. This coarse interval was selected to prioritize the representation of inter-annual persistence of precipitation. For example, two sequential dry years would be more detrimental to glacier mass than the same two dry years separated by a normal or wet year.

We produced 30 realizations of future hourly meteorological time series with the weather generator, representing the most likely factors of change in precipitation and temperature statistical properties and uncertainty related to the stochastic nature of weather and climate. The other meteorological variables required by the hydrologic model (relative humidity, wind speed, short and long wave radiation) were not down-scaled from GCM outputs; rather future changes in these variables were represented through their correlations with and dependence on temperature and precipitation in the weather generator algorithms. We considered a more complex approach based on Monte Carlo analysis to sample from the factor of change PDFs of individual statistical parameters [e.g., *Fatichi et al.*, 2013], but decided against this as it requires an assumption of independence among the statistical parameters (e.g., a change in a parameter in 1 month is independent of the change in others; a change in a parameter is independent among temporal aggregation intervals), and greatly increases the computational burden. While we provide a range of the most probable projections for future watershed processes under a single emissions pathway scenario (RCP4.5), we acknowledge that a much broader range of uncertainty exists in future projections and future work should incorporate ongoing advances in climate modeling, downscaling, multiple emission pathways, and a comparison of multiple hydrologic/glacier modeling approaches, among others, to represent a wider range of uncertainty.

4.4. Model Evaluation Data

Historic remote and in situ measurements of hydroclimatic states and fluxes are critical for model calibration and evaluation. In this study we used glacier mass balance estimated using several methods, glacier surface velocity, glacier discharge, surface energy balance measurements, and satellite-based glacier extent. IRD's glacier monitoring program has made point glacier mass balance measurements on Zongo glacier since the early 1990s. The mass balance data are derived from measurements of a network of stakes in the ablation zone and snow pits in the accumulation zone. These data are available through the Glacioclim database (<http://www-igge.ujf-grenoble.fr/ServiceObs/>). *Soruco et al.* [2009] report time series of cumulative net mass balance of the Zongo glacier estimated from hydrological measurements (discharge and precipitation), glaciological (glacier mass measurements of IRD), and geodetic methods (photogrammetry) which were digitized in this study for model confirmation. Discharge data from a location near the terminus of the Zongo glacier (Tubo, Figure 1) and surface energy measurements were made available by IRD and have been utilized in previous publications [e.g., *Sicart et al.*, 2005, 2011].

Observed glacier extent data are required to evaluate the model's skill in reconstructing rates of recession. We utilized satellite-based estimates of glacier area derived from atmospherically corrected Landsat Thematic Mapper scenes using a Normalized Snow Difference Index (NDSI) threshold following the methods of *Burns and Nolin* [2014]. Images were taken at the end of the dry season, during relatively dry years to avoid mapping snow outside of glacier areas [e.g., *Racoviteanu et al.*, 2008]. 6 Landsat Thematic Mapper scenes were processed and used to analyze glacier recession (2 August 1987, 30 September 1991, 21 June 1995, 3 August 1999, 3 August 2005, and 17 August 2010). The use of Landsat data was preferred over field

measurements of glacier boundaries (which in most years are limited to the lower boundary of Zongo glacier) because the Landsat data are spatially continuous across the entire watershed. The five most recent Landsat-derived ice extent estimates were compared with field measurements of the lower boundary of Zongo glacier. The Landsat derived data are within ± 50 –150 m distance of locally measured terminus positions.

5. Results and Discussion

5.1. Model Evaluation

DHSVM is a physically based model and requires minimal calibration as necessary. Because this study focuses on snow and glacier ice processes, snow roughness length, and snow and ice albedo were calibrated. In addition, to improve model forcing we also selected precipitation and temperature lapse rates through calibration. Here we present optimal parameter values found during calibration (section 3.3) and compare those with values measured at the study location. The optimal values reported in Table 1 are in agreement with previous work and those derived from local measurements. The optimal precipitation lapse rate of $15\% \text{ km}^{-1}$ is within the range derived from weather station observations and high elevation snow pits, 10 – $40\% \text{ km}^{-1}$. The temperature lapse rate ($-8.4 \text{ }^\circ\text{C km}^{-1}$) is stronger than the mean temperature lapse rate of $-5.7 \text{ }^\circ\text{C km}^{-1}$ calculated between the Mevis station (4750 m) and the Off-Glacier station (5050 m) where a mean monthly range of -7.5 to $-4.2 \text{ }^\circ\text{C km}^{-1}$ is observed. The optimal value may be more representative of the distribution of temperature at the watershed scale (elevation ranges 4700–6088 m) than rates calculated from observations at lower elevations or may be compensating for biases in the forcing data. DHSVM decays snow albedo from a maximum value as a function of time after snow fall [Laramie and Schaake, 1972]. The maximum snow albedo we found with calibration is 0.83, consistent with observed values for fresh snow in the area where convective precipitation results in more granular graupel-like snowfall that decreases maximum albedo [Lejeune *et al.*, 2007]. The optimal glacier albedo, 0.39 is slightly greater than that reported by Sicart *et al.* [2011], 0.35. In reality this value is likely to have high spatial variability, whereby high values are observed near the equilibrium line altitude and low values observed near the terminus. An exact match with observational based parameters is not expected as the calibrated parameters will reflect some compensation for any biases in the forcing data, biases in observational data used in calibration, and model construct.

Prior to drawing conclusions as to the role of glaciers in the hydrologic context of the watershed, we evaluated the model's performance in reproducing historical time series of the hydrological and glaciological variables that have been measured in situ. Modeled and observed (reconstructed using hydrological measurements) mean annual net mass balance for the 1987–2006 period were -0.69 and -0.77 (m w.e.), respectively. To confirm the spatial predictions of the model against observations we compared the modeled annual mass balance, reported as the spatial mean within 100 m elevation intervals, with the mean of point measurements for each corresponding elevation range (Figure 3a). For comparison, only elevation intervals with actual measurements (not interpolated measurements) are provided. The model generally reproduced the nonlinear altitudinal gradient in annual mass balance (NSE = 0.75), with some negative biases at lower elevations (Figure 3a).

Differences in the match with the glaciological point measurements are expected as previous studies have demonstrated that the point measurements alone cannot explain net mass balance changes observed using hydrological [Sicart *et al.*, 2005] or geodetic methods [Soruco *et al.*, 2009]. As compared with the other methods of estimating net mass balance of Zongo glacier, net mass balance using interpolated point glaciological measurements underestimates mass losses. Sicart *et al.* [2005] hypothesize that mass losses in steep areas without measurements are higher than those estimated from interpolated measurements because the presence of seracs increases the surface area exposed to melt. Because the source of bias in the glaciological measurements is not entirely clear, the model was not calibrated further as some overestimation of ablation (as compared to glaciological measurements) is required to capture net mass changes of Zongo glacier and discharge observed below the terminus.

Figure 3b shows the cumulative net mass balance of Zongo glacier modeled and reconstructed from hydrological observations and glaciological observations adjusted with geodetic data reported by Soruco *et al.* [2009]. Overall, the model was able to capture the historical trajectory of cumulative net mass changes of

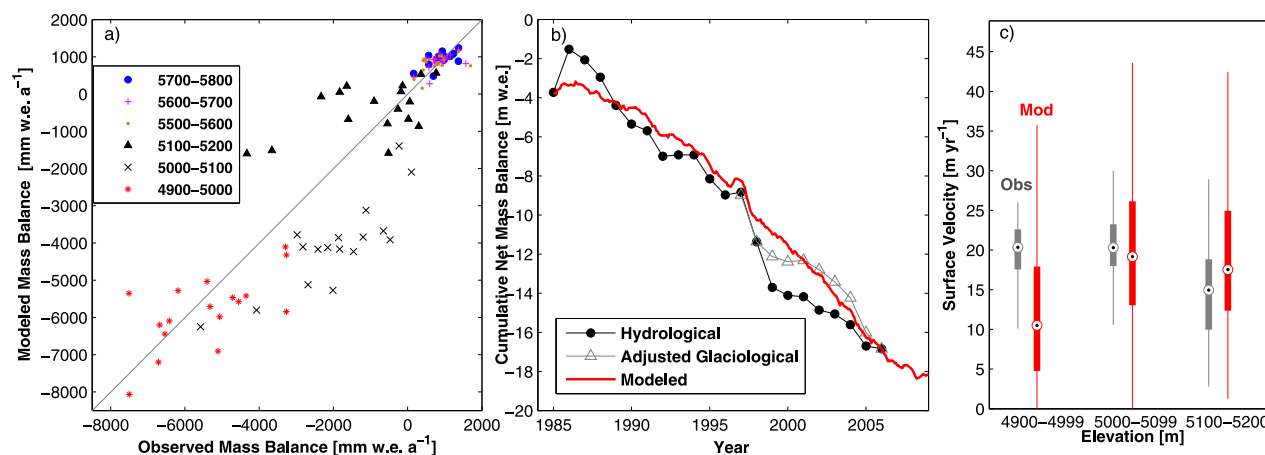


Figure 3. (a) Modeled and annual mass balance plotted for each 100 m elevation interval on Zongo Glacier (1992–2010). (b) Modeled (red), and observed cumulative net mass balance estimated from hydrological measurements (black) and adjusted glaciological measurements (gray). Observations were digitized from *Soruco et al.* [2009]. (c) Box plots showing the distribution of observed and modeled surface velocity in three elevation intervals on the lower reaches of Zongo Glacier. Measured elevation band averaged mass balance and surface velocity data were taken from the Glacioclim database (<http://www-lgge.ujf-grenoble.fr/ServiceObs/>).

the Zongo glacier (Figure 3b). However, the variability of modeled annual mass balance ($\sigma = 0.53$ m) is less than observed using the hydrological approach ($\sigma = 0.74$ m). This is attributed to the reanalysis monthly precipitation time series having lower variance ($\sigma = 0.05$ m) than the observations at the Plataforma location ($\sigma = 0.065$ m, supporting information Figure S5).

As a final step in comparing in situ glaciological measurements on Zongo glacier to predictions of the model, we compared glacier ice surface velocities (Figure 3c). An accurate representation of the velocities in the model indicates that the glacier dynamics algorithms used to evolve glacier area are representative of the actual physical processes. We compared the distribution of measured surface velocities (displacement of stake positions using GPS measurements) with those of the model for three 100 m elevation intervals on the lower reaches of Zongo glacier for the period 1991–2010 (Figure 3c). The modeled surface velocities were calculated by increasing the modeled depth averaged ice velocity by a factor of 1.25 [Cuffey and Paterson, 2010]. The differences between median velocities measured and modeled for the intervals of 5000–5099 m and 5100–5200 m are small, -1.2 and 2.6 m yr^{-1} . There is greater variance in the model estimates as they include every 50 m grid cell in the elevation interval each year, where the measurements are limited to 5–21 measurements across the entire glacier each year. Surface velocities are under predicted in the lowest elevation interval where the modeled median velocity is 9.8 m yr^{-1} less than observed. The total number of observations in this band over the time period is low, 16, while the modeled sample consists of 641 individual annual velocities that may better represent the spatial mean. Additionally, some discrepancies may be introduced by the approximation of ice flow (section 3.1).

In addition to evaluating the simulated changes in mass, we compared the modeled glacier area with estimates derived from satellite imagery over the historical period. Figure 4 shows the predicted ice thickness (ice water equivalent, IWE, m w.e.) and extent and satellite derived glacier extent at the start of the historical period (1987 plot a), in 1999 (plot b), and at the end of the historical period (2010, plot c). The general pattern of areal retreat is reproduced by the model across the watershed. Nonetheless, there are some inconsistencies in the simulated and satellite-derived extents. The ice mass near the southwest perimeter retreated significantly in the satellite-derived data, but not in the model (see Figure 4c indicated with an arrow). Also, the tongues of the small glaciers located on the eastern side of Huayna Potosi do not shrink as they do in the Landsat derived data. Several aspects of the modeling approach could explain these shortcomings. The model lacks a representation of reflected and emitted longwave radiation from surrounding terrain that could be a significant source of heat to the margins of valley glaciers [Sicart et al., 2011]. Another model limitation that could lead to mismatch in the glacier boundaries is that the SEB parameters are spatially uniform. In steep mountain regions where erosion may be active, changes in snow and ice surface albedo may result from sediment deposition, which is not incorporated in the current model. Lastly, the method of initializing the glacier ice distribution (section 3.2) introduces some uncertainty. The actual state

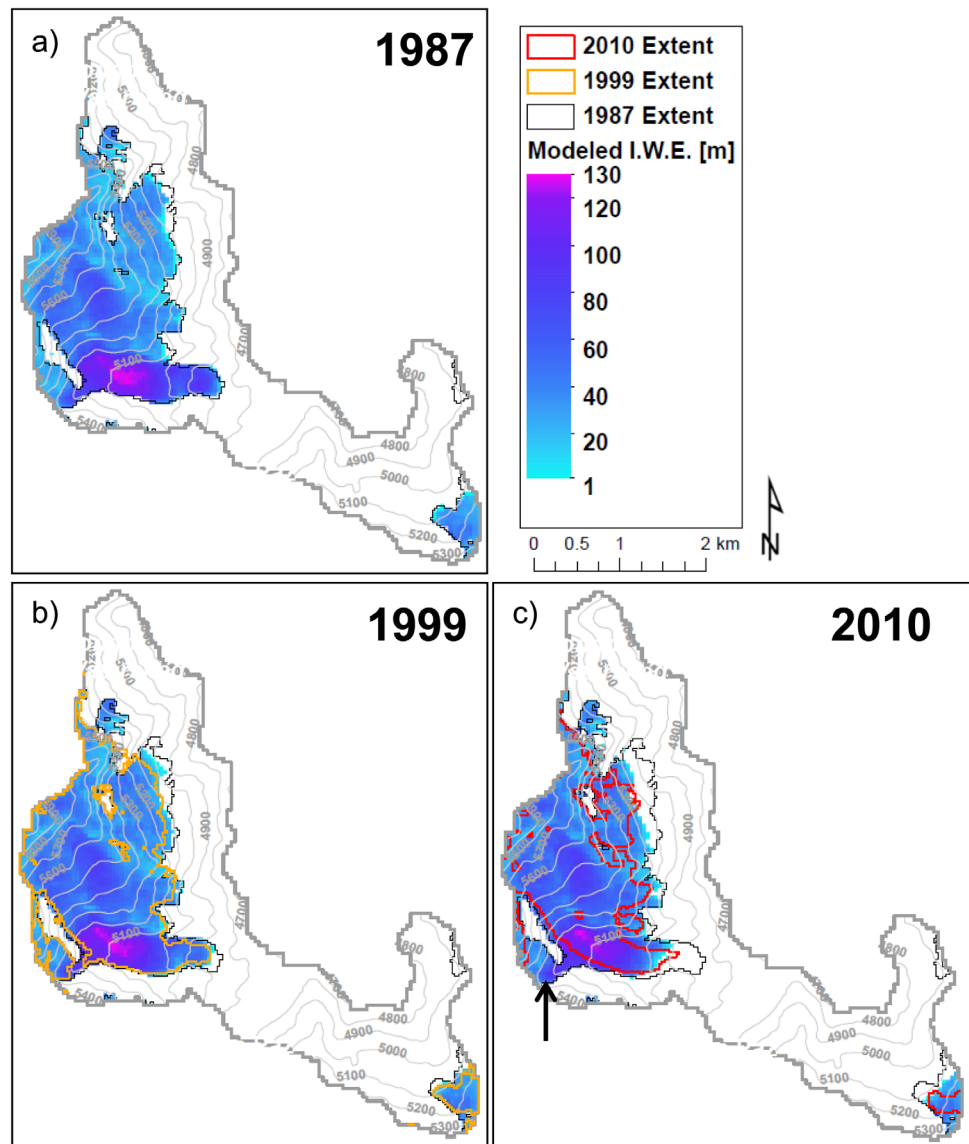


Figure 4. Modeled ice water equivalent (IWE) for (a) 1987, (b) 1999, and (c) 2010. Satellite derived estimates of glacier area are shown with the thin solid black (1987), yellow line (1999), and red line (2010). The arrow indicates an area of significant mismatch between modeled and observed extent.

of the glaciers in the mid-1980s was a product of a long period of climate fluctuations which was not explicitly used to spinup the glacier masses due to limited knowledge of long-term climate forcing.

More complex models of ice flow can be used to predict glacier evolution. However, in this implementation we preferred to use a simplified glacier flow model suitable for watershed to regional scale predictions [Clarke *et al.*, 2015]. Réveillet *et al.* [2015] implemented a highly sophisticated full-Stokes model to simulate ice flow of Zongo glacier. Our modeled historical ice thickness distribution (Figure 4) compares well with the boundaries, and the general spatial patterns predicted in Réveillet *et al.* [2015, Figure 3]. For example maximum modeled ice thickness in 1997 is 132 m for this study, corresponding to 120 m in the same area of the glacier for Réveillet *et al.* [2015].

A time series of discharge measured below the terminus of the Zongo glacier at the Tubo site (Figure 1) was used to evaluate the simulated discharge volume. At this measurement point the upslope contributing area covered by glacier ice varied between 75% in 1987 and 55% in 2010. Therefore model predictions at this point largely demonstrate the model’s performance in predicting flows driven by snowmelt, glacier

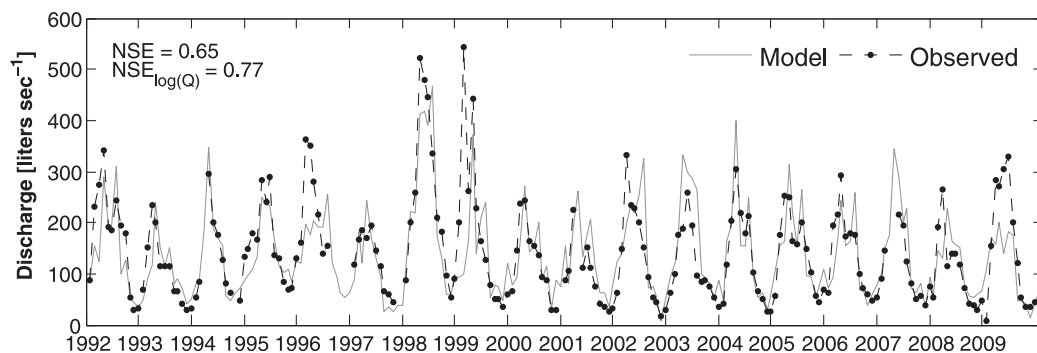


Figure 5. Simulated and observed monthly mean discharge at the measurement location below the terminus of Zongo glacier. Discharge measurements that contain periods of missing data were removed from the calculation of mean discharge values. Year ticks signify 1 September of the labeled hydrological year.

melt, and rain driven runoff. Figure 5 shows the monthly mean modeled and observed time series of discharge for hydrological years 1992 through 2010. Average annual flow ($\mu_{obs} = 150$ l/s) and flow variation ($\sigma = 99$ l/s) match well ($\mu_{mod}/\mu_{obs} = 0.98$; $\sigma_{mod}/\sigma_{obs} = 0.93$). Besides these statistical comparisons, the NSE of 30 day mean discharge and natural log of discharge (which is more sensitive to low flows) are calculated as 0.65 and 0.77, respectively, indicating a “good” performance rating following the widely accepted model evaluation guidelines of *Moriasi et al.*, [2007]. The model was able to capture the seasonal and inter-annual variability of discharge; however its skill was less at shorter time scales (submonthly). Several elements of the model application contribute to this shortcoming. First, short-term model error is likely dominated by the inaccuracy of the meteorological forcing data. The historical data were derived from reanalysis products with a coarse spatial resolution ($1/2 \times 2/3^\circ$) that was bias corrected using local data (section 3.4). Therefore, while systematic seasonal and diurnal biases are removed, local hydrologic behavior attributed to “event” time scales (days to weeks) are not likely to be reproduced accurately. This likely is the largest source of error. Also, while storage/release and refreezing of melt water is explicitly represented in the modeled snow layers, the model does not represent englacial and subglacial routing of melt water through the glacier ice layer [*Naz et al.*, 2014]. A small proglacial lake between the glacier terminus and gauge location developed as the glacier retreated. This lake likely has some influence on storage and routing of discharge. The lack of these processes in the model limits the accuracy of the timing of simulated discharge at short time intervals, but is not reflected in the accuracy of the seasonal and long term projected runoff, which are generally well simulated.

We also compared the modeled mean monthly land surface energy fluxes with local measurements [*Sicart et al.*, 2005] conducted during the hydrological year of 2000 at an elevation of 5050 m on the Zongo glacier. 1 : 1 plots comparing monthly fluxes and a bar plot with modeled and observed net shortwave radiation (SW, incoming minus reflected), net longwave radiation (LW, downward minus emitted), sensible heat (SH) and latent heat (LE) exchanges is shown in Figure 6. A positive (negative) flux represents net energy gain (loss) at the glacier surface. While there are uncertainties in the measurement of these variables [*Helgason and Pomeroy*, 2012; *Lundquist et al.*, 2015], as well as complications in the comparison of measurements at a point with fluxes simulated over the model’s 50 m grid cell, the simulated and measured seasonality of energy exchanges are in agreement (Figure 6e). However, large biases are apparent in shortwave radiation late in the wet season (MAM), which is heavily dependent on cloud cover (represented in model forcing) and albedo (represented in snow model algorithms and parameterization), and has the greatest nonseasonal variability. This positive bias in SW can be linked to over-predicted discharge at the end of the wet season in some years (e.g., 2000, 2006; Figure 5). The highest bias is in the losses of latent heat (sublimation) during the months of the dry season which may lead to positive biases in energy simulated at the snow/ice surface during these months. This bias in the exchange of latent heat is likely linked to a simplified formulation for the correction for atmospheric stability utilized in the model [*Andreadis et al.*, 2009], inaccuracies in wind speed and relative humidity used as model forcings, and the lack of a representation of seasonally varying aerodynamic roughness length over snow/ice [*Wagon et al.*, 1999], which is reduced to a constant in the model, and uncertainty in the measurement of daily sublimation with rudimentary lysimeters [*Wagon et al.*, 1999; *Sicart et al.*, 2005].

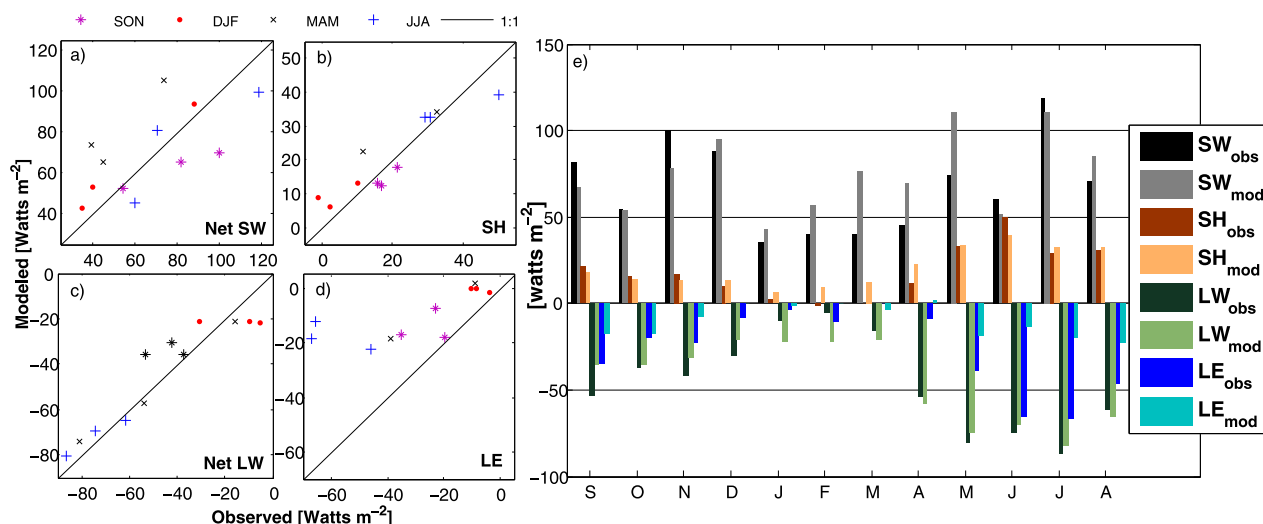


Figure 6. Modeled (mod) and observed (obs) surface energy fluxes (monthly averages) at 5050 m a.s.l. on Zongo glacier for the hydrological year 1999/2000: (a–d) 1 : 1 plots showing model performance; (e) plotted as monthly time series to show seasonal dynamics. Observations are taken from *Sicart et al.* [2005]. Turbulent fluxes were not measured during March.

This bias in net shortwave radiation and latent heat can be reduced by calibrating the model against the point-scale fluxes measured in the field. We conducted point scale calibrations where the decay of snow albedo was modified and a representation of seasonal katabatic cooling of air temperature over glacier surfaces was included. To represent the latter, near surface air temperature on the glacier was decreased (with respect to the interpolated value from the off glacier station) based on a comparison of on and off glacier measurements of temperature at locations with the same elevation (5050 m, Figure 1). The seasonal variability of the differences between on and off glacier mean monthly temperature ranges from 0 in January, when there is no clear difference observed, to 2.4°C in June where near surface air temperature is lower on the glacier. This model configuration decreased MAM net shortwave radiation by 11% and increased sublimation (negative latent heat flux) by 70%, reducing model biases to some extent. While fine-tuning of the model provided improved predictions at the point scale, when the model was run at the watershed scale with point-calibrated parameter values, model skill for predicting glacier extent, mass balance, and discharge lessened. Because the goal of this paper is to examine watershed-scale predictions, it was deemed relevant to use model runs with watershed-scale calibration.

5.2. Historical Model Application

We ran the model using the historical bias-corrected NASA-MERRA data from 1987 to 2010 to examine and quantify the glacio-hydrologic response to historical climate. The definition of glacier melt has varied in the literature [see *La Freniere and Mark, 2014*] while some define the glacier contribution as all the water leaving the glacier footprint, including snowmelt and rain falling on the glacier [e.g., *Mark and Seltzer, 2003; Gascoign et al., 2011*], others include only the melting of glacier ice [e.g., *Stahl et al., 2008; Favier et al., 2009; Ragettli and Pellicciotti, 2012; Immerzeel et al., 2013*]. The choice of definition is largely constrained by the method of analysis. Whereas some modeling approaches can more easily separate water sourced from snow and ice, many field measurement approaches cannot easily differentiate the two. We use the latter definition, as in many high alpine watersheds snowmelt will continue to be an important component of the water balance for some time after glaciers have receded.

To describe the role of glaciers in watershed discharge we analyzed the modeled discharge entering the reservoir, which collects runoff from the entire catchment through the canal system (Figure 1). Measurements of all the discharge entering the reservoir are not available for use in this study for model confirmation. Therefore, we rely on the model confirmation reported in Figure 5 to justify the use of this model for predictions at the catchment scale. Historically (1987–2010), on average the modeled glacier melt represents 27% of annual discharge in the watershed (Figure 7a). This contribution is enhanced during the dry season (JJA), 61% (on average), when seasonal precipitation is at a minimum. The quantity and relative contribution of glacier melt is reduced in wet years (e.g., WY 2008, Figure 7b) when fresh snow cover provides

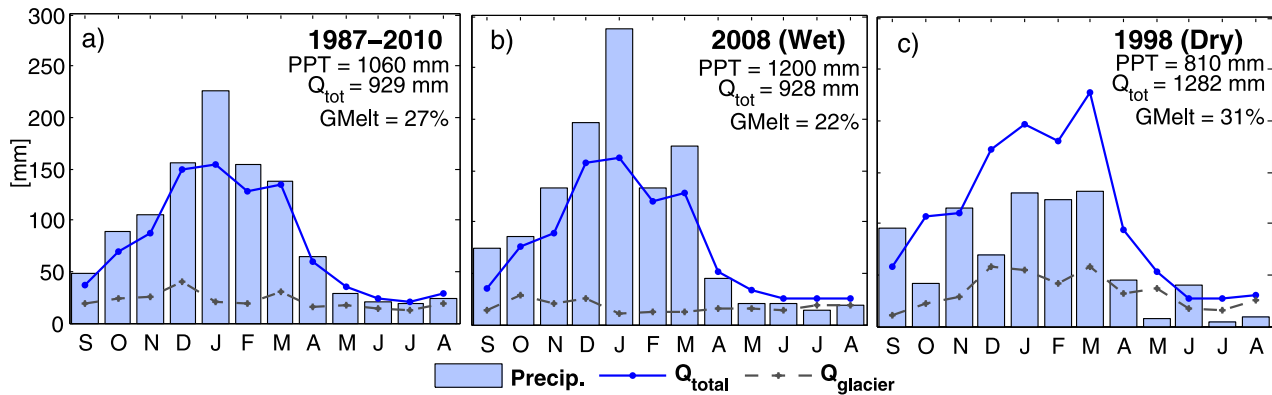


Figure 7. Monthly mean precipitation (bars), modeled total discharge (blue, solid line) entering the reservoir, and glacier melt (gray, dashed line) plotted for: (a) the historical period (1987–2010); (b) a wet year (2007–2008); and (c) a dry year (1997–1998). In the inset annual precipitation (PPT), runoff (Q_{tot}), and percent of glacier melt contribution (%GMelt) are reported.

an albedo feedback that increases the reflection of shortwave radiation at the surface and reduces melt. Glacier melt discharge increases substantially in dry years (e.g., 1998, Figure 7c). For example, during the El Niño event of 1998, when warm and dry conditions persisted during the wet season (summer, DJF), the glacier melt contribution was 34% during January, compared to a long-term (1987–2010) average of 13% for the same month. During January, fresh snowfall usually results in minimum melting at the glacier surface and accumulation at high elevations. In El Niño years discharge was further enhanced by the melting of accumulated snow at higher elevations in the watershed as reflected in the catchment mean monthly hydrograph (Figure 7c). During these years discharge can exceed precipitation.

5.3. Hydrologic Response to Glacier Recession Through the 21st Century

We conducted simulations forced with 30 realizations of the future climate (as described in section 3.4). These realizations reflect inter-annual variability in temperature and, on average, predict a warming of approximately 3°C by the end of the century (Figures 8a, and 8b), consistent with previously reported estimates for the region from GCM outputs [Bradley et al., 2006; Vuille et al., 2008]. While annual precipitation is

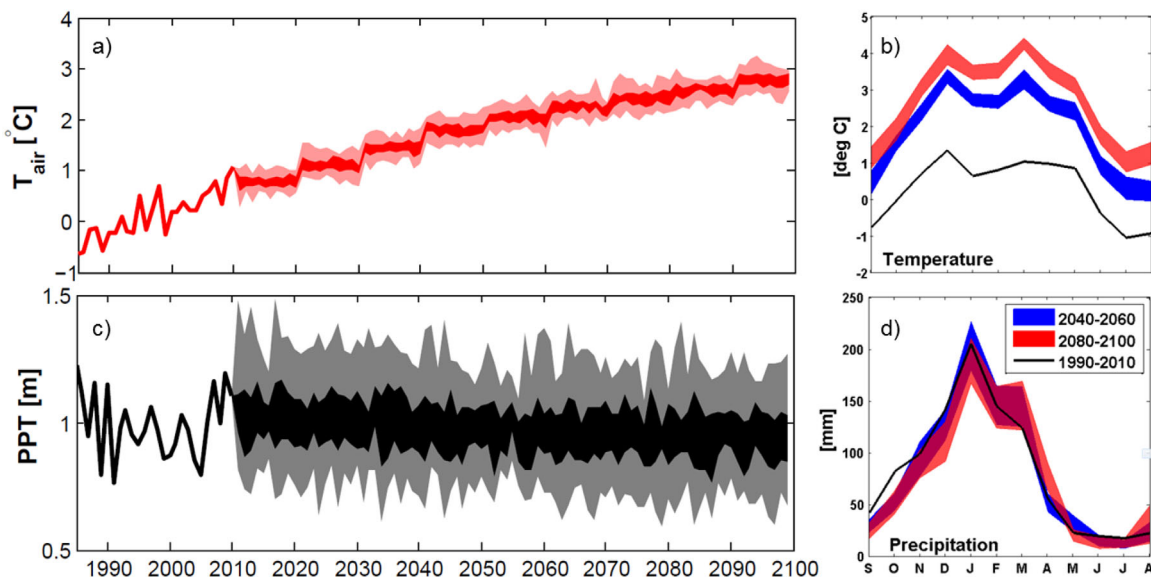


Figure 8. (a) Historical and projected annual mean air temperature and (c) annual precipitation. The full range of values reflect variability represented through statistical downscaling, while the darker regions represent the interquartile range of the projections. The seasonality of (b) air temperature and (d) precipitation is shown for the historic time period (1990–2010, black line), the near future (2040–2060, blue), and the far future (2080–2100, red). The ranges represented for the time periods reflect the ranges in mean monthly values of the future realizations. The data reflect the elevation of the meteorological station used in the analysis (5050 m a.s.l.).

highly variable, the average over all of the future realizations indicates an 8% decrease in annual precipitation by the end of the century (Figure 8c), mostly attributed to reduced precipitation during the transitional period prior leading into the wet season (Figure 8d). This result is consistent with predictions of wet season precipitation projected by regressing future GCM zonal flow patterns, (generally accepted to be accurately simulated by GCMs; see *Christensen et al.* [2007] and *Luce et al.* [2013]) with precipitation station observation locations [*Minvielle and Garreaud*, 2011] and end of century projections of precipitation using a higher resolution regional climate model [*Urrutia and Vuille*, 2009]. Nonetheless, it should be emphasized that there is considerable uncertainty in predictions of future precipitation [*Buytaert et al.*, 2010].

To examine the response to the future climate at the watershed scale, we evaluated the progression of glacier mass and area. For future projections we report the mean and range (in parentheses) of the ensemble of 30 future stochastic climate realizations. With respect to the initial state in 1987, the glacier area and volume are projected to decline 50(48–53)% and 61(60–66)% by 2050 and 73(71–77)% and 81(79–84)% by end of century, respectively. Figure 9 shows the mean predicted distribution of glacier ice in the watershed for years 2040, 2060, 2080, and 2100. While the glaciers do not completely disappear, their termini retreat to higher elevations. On average the terminus of the Zongo glacier is projected to retreat 1.9 km to an elevation of ~5300 m in 2100. This is a sharp contrast to beginning of the historical period when the glacier extended to 4850 m.

To determine how the evolving change in glacier area will affect discharge seasonality, we composited mean monthly flows of total runoff and glacier melt and their % change with respect to the historical period into two periods, the near future (2030–2050) and late century (2080–2100) plotted in Figure 10. The ranges of future data reflect the variability of climate represented through the multiple stochastic realizations of future meteorological forcing. In the near future, discharge entering the reservoir is expected to decrease during dry months, with the largest decreases occurring in August, 30(21–39)% less than the 1987–2010 mean. Midcentury, wet season discharge is predicted to increase. As temperatures rise, high elevation areas that historically accumulated snow (which would eventually densify to glacier ice) contribute more to runoff through increased transient snowmelt and rainfall at the expense of mass accumulation. At the end of century, watershed discharge is projected to continue to decline throughout the year, with dry season (JJA) flows declining by 57% on average and the glacier melt contribution becoming negligible (Figures 10b and 10d). Annual runoff is predicted to change $-4(-15 \text{ to } 2)\%$ and $-24(-33 \text{ to } -18)\%$ for the mid and late century time periods. These declines are linked to declining contributions of glacier melt associated with loss of area; however decreases in precipitation leading into the wet season and increased evapotranspiration also play a significant role. Late century, increased evapotranspiration and decreased precipitation largely offset runoff gains from high elevation areas that transitioned from zones of snow accumulation to snowmelt and rain dominated zones earlier in the century.

To identify the temporal patterns in the continuous hydrologic response to glacier change, we tracked the progression of total watershed runoff and glacier melt annually and during the dry season (JJA) between 1987 and 2100 in Figures 11a and 11b. Both annual and dry season runoff showed a pattern of increase until around 2010 and are predicted to decrease sometime within the following decade. Dry season runoff declines steadily until the second half of the century when the glacier contribution tapers to a minimum (Figure 11b). The mean of the coefficient of variation (CV) of dry season flow for all future climate realizations (calculated using a moving 30 year window) steadily increases from 0.23 over the historical period to 0.49 at the end of century. This increased variability is linked to (1) decreasing contribution from glacier melt in sustaining low flows; and (2) precipitation events during the dry season (albeit small in magnitude and less frequent) occurring as rain rather than snowfall over larger areas of the watershed. On average the change in CV of annual flows is small, increasing from 0.1 to 0.13 over the course of the 21st century. Likewise, CV of annual precipitation shows no clear temporal pattern (range of 0.14–0.15 throughout the period). Historically, the largest annual flows were attributed with dry and warm years (El Niño) where snow and ice stored in the watershed had a large contribution to runoff. These high annual flows decrease in time as the amount of ice and snow stored in the watershed is reduced.

As described above, changes in glacier melt have a strong influence on temporal patterns of watershed discharge. Concurrent with these changes, the relative contributions of snowmelt and rain and losses through evapotranspiration will evolve with the changes in climate. The progression of these fluxes at the annual time scale, and composited seasonally for the historical period, midcentury, and late century

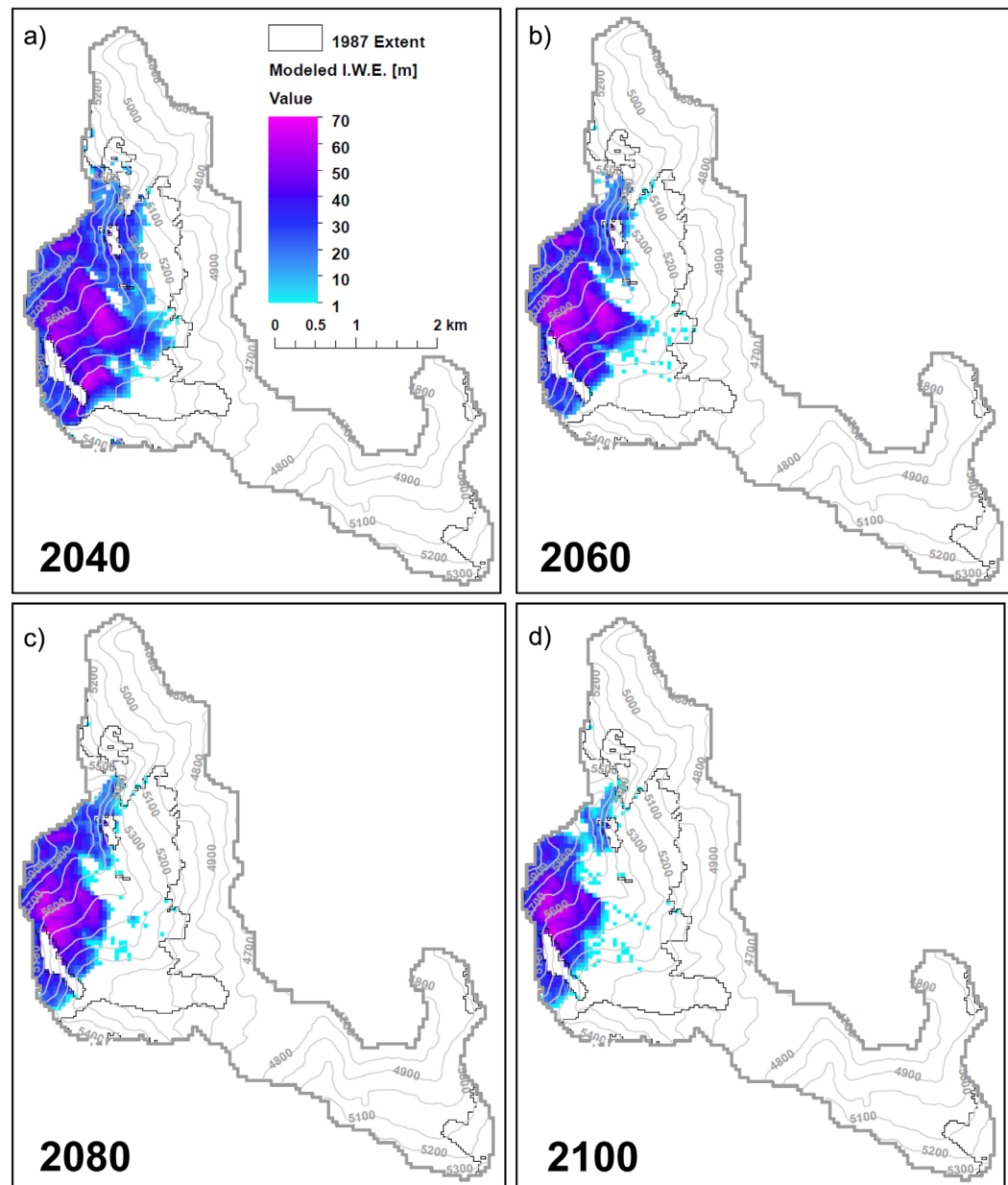


Figure 9. Projected glacier area and thickness at the end of 2040, 2060, 2080, and 2100. Satellite derived glacier extent estimates for 1987 are shown with a black outline.

is shown in Figure 12. The fluxes entering the watershed (snowmelt, rain, glacier melt) do not include the effects of any losses through watershed processes (e.g., evapotranspiration, soil moisture storage). In contrast, runoff plotted in Figures 10a, 10b, and 11 shows the glacier melt component of stream discharge generated in the watershed which includes the effects of these losses by routing the mass through the watershed. Unlike the trajectory of changes in glacier melt, changes in rain, snowmelt and evapotranspiration show patterns of change (Figure 12a) that closely reflect increasing air temperature (Figure 8a). In addition to reductions in runoff input from declining glaciers with climate change, the growing amount of evapotranspiration from November to the end of March leads to significant losses of annual runoff. As air temperature gradually warms above the freezing point (at the 5050 m reference location) evapotranspiration losses increase, by as much as 86% by the end of century. This demonstrates the importance of the response of the nonglacierized portions of the watershed for predicting future runoff patterns in a warming climate.

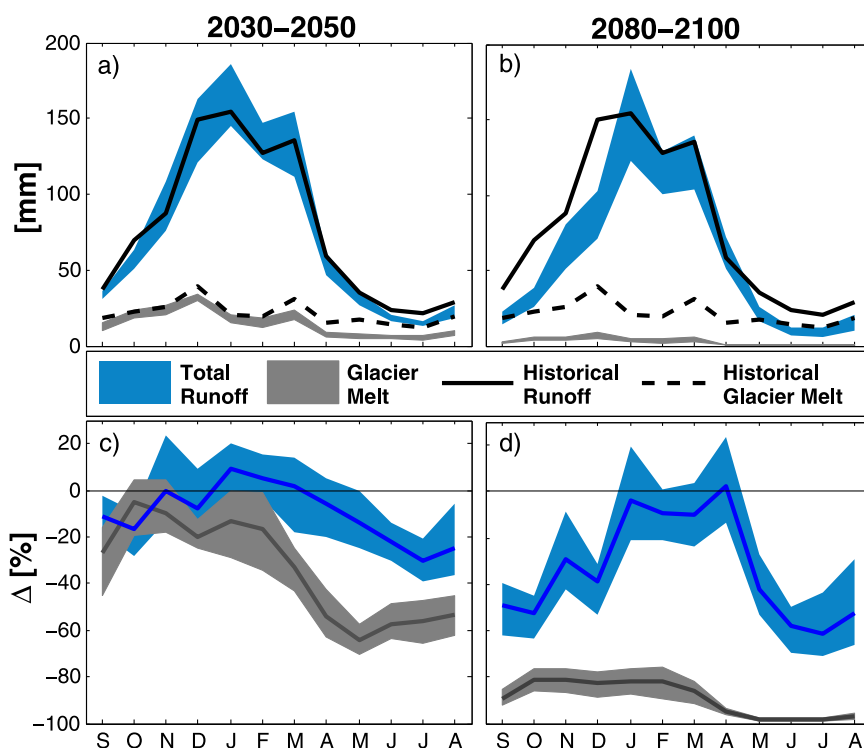


Figure 10. Mean monthly runoff (sourced from rain, snowmelt, and glacier melt) entering the reservoir predicted for (a) the near future (2030–2050) and (b) far future (2080–2100). Percent change relative to 1987–2010 in total runoff and glacier melt for the (c) near and (d) far future. Mean values of percent change (with respect to historical) between scenarios are indicated by the dark solid lines.

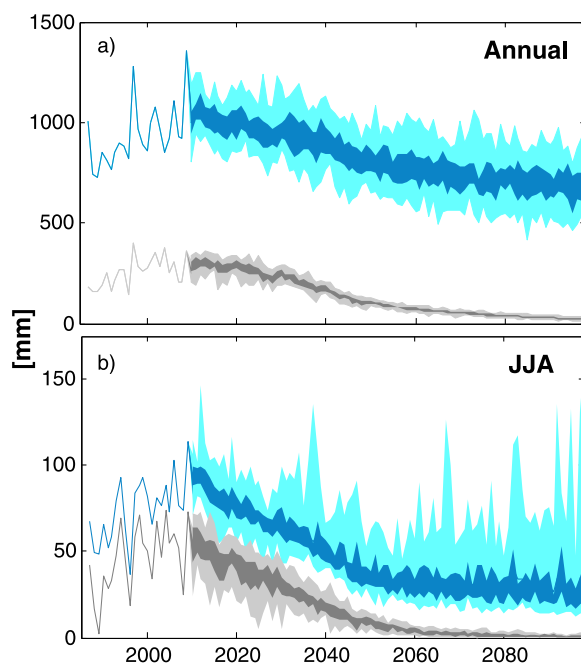


Figure 11. (a) Annual and (b) dry season (JJA) total runoff (rain + snowmelt + glacier melt, blue) and glacier melt (gray) for the entire watershed. Lighter colors indicate the full range of future projections using multiple stochastic realizations of the transient future climate and dark colors denote the interquartile range of the projections.

Aside from the influence of snow cover on glacier melt and mass evolution, the transition of snowmelt to rain-derived discharge does not have a large influence on seasonal redistribution of water. In contrast to temperate mountainous watersheds, in high altitude tropical watersheds snow cover outside of glacier areas and at lower elevations on glaciers is often transient, melting within days of falling. This prevents the development of a snowpack and leads to small time lags between snowfall and runoff events [Lejeune *et al.*, 2007]. For this reason, a transition from snowmelt to rain-derived discharge plays a lesser role in major seasonal changes in discharge patterns.

5.4. The Role of Glacier Dynamics and Parameter Selection in Model Projections

In many mountainous watersheds, observational data sets are unavailable or are of short duration which makes model parameter selection and model calibration very difficult. This leads modelers to select parameters based on values reported in the literature or extrapolate parameters from other regions.

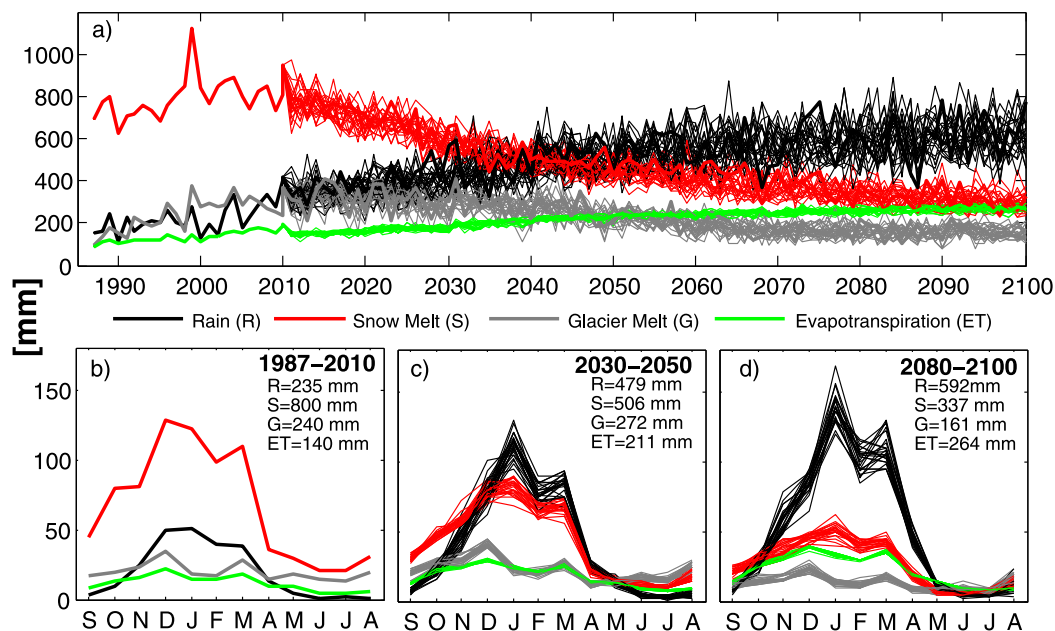


Figure 12. Historical and projected (a) annual and (b–d) seasonal fluxes of rain, snow melt, glacier melt, and evapotranspiration (ET) in the watershed.

To examine the sensitivity of the glacio-hydrology model to model configuration and parameter selection, we compared the results from calibrated parameters presented above with alternate configurations (i.e., no glacier flow and with creep and basal sliding in the glacier model) and ranges of SEB and climate parameters that are physically plausible for this study location. To facilitate this comparison we compared modeled glacier area (Figures 13a–13g) and dry season (winter, JJA) runoff (Figures 13h–13n) from 1987 to 2100. JJA runoff was selected as it is most sensitive to changes in glacier area. It is presented as a 10 year centered running mean for clarity. A single realization of the future climate is used for the projected time period. This analysis reflects model sensitivity, not parameter uncertainty. In most cases the evaluated parameters were not be able to reproduce historical hydroclimatic patterns as accurately as the calibrated parameters.

We first analyzed the role of glacier dynamics. The model uses a vertically integrated shallow ice approximation which simulates creep, but we have neglected the influence of basal sliding due to uncertainties in its parameterization for all glaciers in the watershed (section 3.1). We compared this assumption with a model configuration that neglects ice flow all together (no lateral movement of ice, Static) and one that includes basal sliding in addition to movement through creep (Creep + Sliding). Neglecting ice flow leads to more rapid retreat (Figure 13a) as ice at lower elevations is not replenished by ice flow from higher elevations. This in turn leads to less of an increase in JJA runoff early in the 21st century (Figure 13h). When dynamics are represented, a much larger peak in runoff is observed because ice flow allows the ice bodies to sustain for a longer duration at lower elevations with warmer air temperatures. Late in the 21st century the static case has more glacier area and JJA runoff because mass accumulated at higher elevations earlier in the time period was not redistributed to lower elevations. In the configuration that considered basal sliding, the sliding law coefficient (C , equation (2)) was set to $2.0 \times 10^{-11} \text{Pa}^{-2} \text{yr}^{-1}$, the upper limit in the range presented by Clarke *et al.* [2015]. The inclusion of this configuration of basal sliding resulted in negligible differences in modeled glacier area (Figure 13a). This formulation increased mean surface velocities below 5200 m $0.3\text{--}1.8 \text{ m yr}^{-1}$ during the historical period. Based on this analysis and the agreement with surface velocities when basal sliding is neglected (Figure 3c) it is likely that the role of basal sliding is low during this period of retreat.

Next, we explored SEB and climate parameters that have significant influence on rates of ablation (Figures 13b–13f and 13i–13m). We evaluated the projected response using different values of glacier albedo, maximum snow albedo, aerodynamic roughness length over snow and ice, and the precipitation and temperature lapse rates. For each case only the parameter being analyzed is altered, all other parameters remained

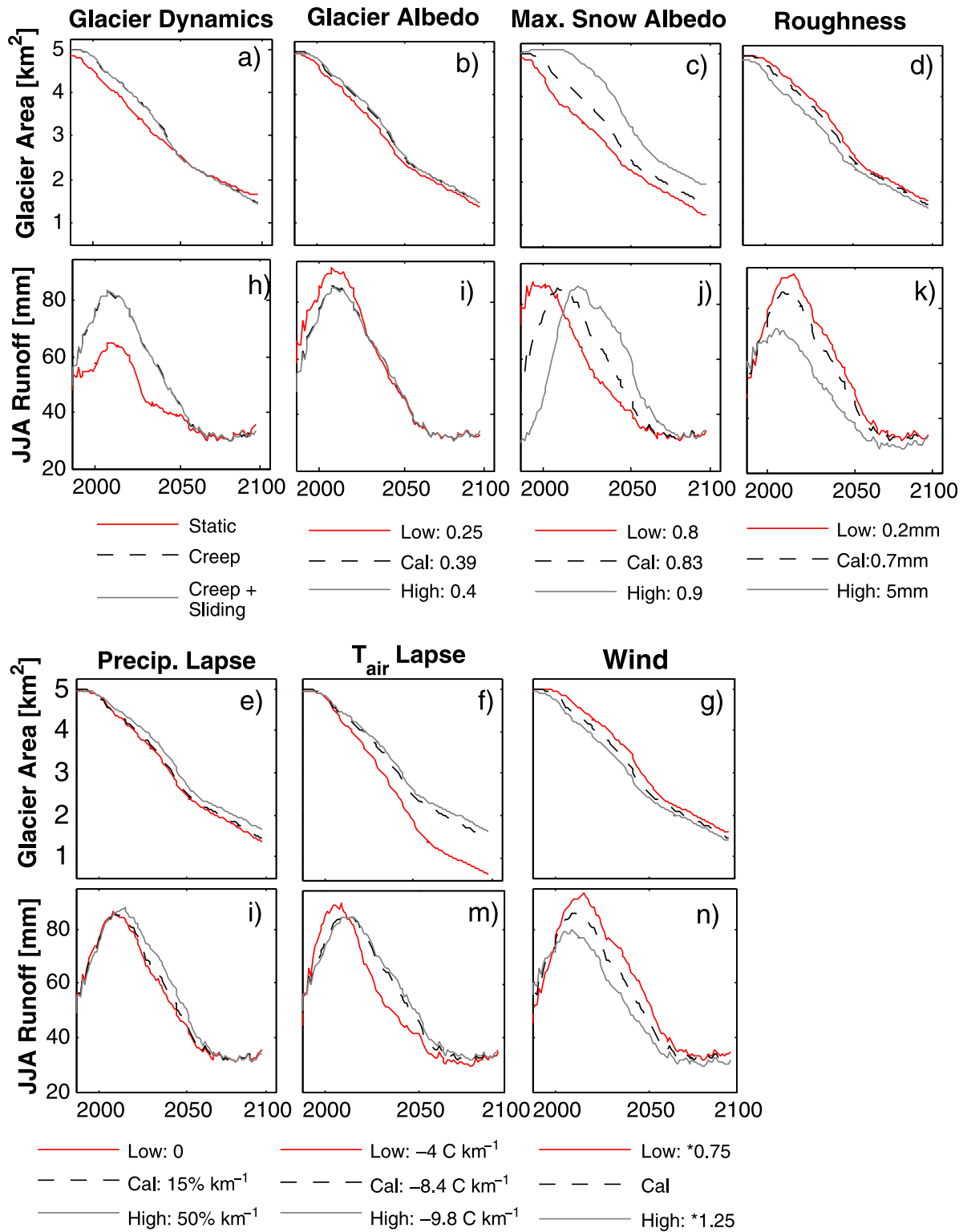


Figure 13. Sensitivity of (a–g) glacier area and (h–n) JJA runoff to different model configurations and parameter selection for a single future climate realization. The optimal parameter value (Cal) was found through multiobjective calibration while the low and high values represent physically plausible end members for the region. A wind multiplier was not used in calibration however a range was tested for this analysis. The results reflect the 10 year centered mean of simulations using a single climate forcing realization.

at their calibrated values and the ice flow configuration utilized the creep only case. In most cases, differences between selected parameters were most pronounced for the evolution JJA runoff in the early part of the 21st century (Figure 13). Later in the century glacier ice is limited to high elevation areas and does not contribute a significant amount of melt during the dry season.

While the other parameters largely controlled the magnitude of dry season discharge response, maximum snow albedo greatly changes the rate of retreat (Figure 13c) which leads to temporal shifts in the response of JJA runoff, while the magnitude and shape of response remains intact. Decreasing maximum albedo to 0.8 (calibrated = 0.83) results in peak dry season runoff response occurring approximately a decade earlier. Increasing this value to 0.9 delays retreat until 2009 shifting peak runoff response to a decade later. Increasing aerodynamic roughness length to 5 mm (calibrated = 0.7 mm) promotes sensible and latent heat exchanges at the glacier surface, leading to increased recession and initial increased runoff. Applying a single value to both snow and ice may be problematic [Brock *et al.*, 2006]. Selecting realistic ranges for each surface individually would likely narrow this range in response. The temperature lapse rate determines the elevation of the zero degree isotherm. Increasing this value amplifies the sensitivity of higher elevation areas to rising temperatures leading to more rapid recession. These findings are consistent with those of Ragetti and Pellicciotti [2012] who found temperature lapse rate and an empirical solar radiation parameter to be the most sensitive in a glacio-hydrological model application in central Chile.

Wind speed was bias corrected using local observations at the Off-Glacier station where there is a complete data set with all of the required variables (section 4.2) and treated as a spatially homogenous field throughout the watershed. Wind speed is likely to vary across the landscape and it is uncertain whether the station we used for bias correction is representative of an average value for the entire basin. For example, during the period of 2004–2009, the mean wind speed at this location (2.86 m s^{-1}) was 18% higher than that observed at the On-Glacier measurement location (2.42 m s^{-1} , Figure 1). To test potential uncertainties associated with this assumption we increased and decreased wind by 25%. Decreasing wind speed decreased glacier melt and recession, while increasing wind speed had the opposite effect. This leads to approximately 7 year difference in the timing of peak response and a 16% difference in peak magnitude within the range evaluated. These responses are dependent of the calibrated roughness length value. The optimal value of roughness length (0.7 mm) is on the lower end of the range of measurements reported by Brock *et al.* [2006]. This may reflect compensatory effects for a positive bias in wind speed with respect to a field that would more representative of the entire watershed.

6. Conclusions

In partially glacierized watersheds climate change can yield highly complex glacio-hydrologic responses over time. Understanding and predicting the different factors that control such behavior is of paramount importance in regions where the aquatic environment and anthropogenic systems rely on glacier melt water. In this study we improve the understanding of the complex response of a partially glacierized watershed within the context of the headwaters of the Zongo River in Andean cordilleras of Bolivia. Driven by retrospective and future climate forcing our glacio-hydrologic model analysis provide the following general results:

1. Considering glacier ice dynamics in a distributed hydrology model is crucial for predicting the climate change impacts in partially glacierized watersheds.
2. The skewed shape of runoff response with time is controlled by the interplay between temporally varying positive and negative trends in glacier ice melt, and the positive trend of evapotranspiration under a warming climate.
3. Increased evapotranspiration from nonglacierized areas will have an increasing influence on water availability with rising temperatures and is an essential component to consider in long-term projections.
4. The buffering effect of glacier melt on low flows will diminish in time, increasing variability during the dry season. Identifying increases in flow variability as flows decline is critical for water management purposes.
5. Calibration and selection of SEB and climate model parameters plays a significant role in model projections of glacier area and runoff patterns. Long-term projections are highly sensitive to selection of maximum snow albedo, surface roughness, and temperature lapse rate.

This study demonstrates the potential of applying advanced process based simulation models for prediction of future water availability in partially glacierized river basins. Parameter sensitivity analyses provide a cautionary example of the potential for a high degree of uncertainty in future projections when applying such complex models in areas that lack local data to properly constrain model parameter selection and model calibration. This underscores the importance of long-term field measurement programs, such as the GLACIOCLIM Observatory on the Zongo site to guide and provide a basis for modeling efforts.

Acknowledgments

The Modern Era Retrospective-analysis for Research and Applications (MERRA) reanalysis meteorological data can be downloaded from the Goddard Earth Sciences Data and Information Services Center (GES-DISC, <http://disc.sci.gsfc.nasa.gov>). Most of the glaciological and meteorological data measured in the watershed that were utilized in this study can be downloaded from the Glacioclim database (<http://www-igge.ujf-grenoble.fr/ServiceObs/>). Nonpublic glaciological and meteorological data can be obtained with agreement from the Institute of Research for Development (IRD). The CMIP5 general circulation model output can be downloaded from the World Climate Research Program (WCRP, <http://cmip-pcmdi.llnl.gov/cmip5/>). The Landsat Thematic Mapper scenes can be downloaded from the United States Geological Survey (USGS, <http://earthexplorer.usgs.gov/>). All glaciohydrological model data presented in this manuscript are available by request through the corresponding author (chrisf2@uw.edu). Surface energy balance observations were provided by Jean Emmanuel Sicart (jean-emmanuel.sicart@ird.fr). This research was supported by the NASA Interdisciplinary Research in Earth Science Program grant NNX10AP90G.

References

- Adhikari, S., and S. Marshall (2012), Glacier volume-area relation for high-order mechanics and transient glacier states, *Geophys. Res. Lett.*, **39**, L16505, doi:10.1029/2012GL052712.
- Andreadis, K. M., P. Storck, and D. P. Lettenmaier (2009), Modeling snow accumulation and ablation processes in forested environments, *Water Resour. Res.*, **45**, W05429, doi:10.1029/2008WR007042.
- Baraer, M., B. G. Mark, J. M. McKenzie, T. Condom, J. Bury, K. Huh, C. Portocarrero, J. Gómez, and S. Rathay (2012), Glacier recession and water resources in Peru's Cordillera Blanca, *J. Glaciol.*, **58**(207), 134–150.
- Barnett, T. P., J. C. Adam, and D. P. Lettenmaier (2005), Potential impacts of a warming climate on water availability in snow-dominated regions, *Nature*, **438**(7066), 303–309.
- Berg, A. A., J. S. Famiglietti, J. P. Walker, and P. R. Houser (2003), Impact of bias correction to reanalysis products on simulations of North American soil moisture and hydrological fluxes, *J. Geophys. Res.*, **108**(D16), 4490, doi:10.1029/2002JD003334.
- Bradley, R. S., M. Vuille, H. F. Diaz, and W. Vergara (2006), Threats to water supplies in the tropical Andes, *Science*, **312**(5781), 1755–1756.
- Brock, B. W., I. C. Willis, and M. J. Sharp (2006), Measurement and parameterization of aerodynamic roughness length variations at Haut Glacier d'Arolla, Switzerland, *J. Glaciol.*, **52**(177), 281–297.
- Burns, P., and A. Nolin (2014), Using atmospherically-corrected Landsat imagery to measure glacier area change in the Cordillera Blanca, Peru from 1987 to 2010, *Remote Sens. Environ.*, **140**, 165–178.
- Buytaert, W., M. Vuille, A. Dewulf, R. Urrutia, A. Karmalkar, and R. Celleri (2010), Uncertainties in climate change projections and regional downscaling in the tropical Andes: Implications for water resources management, *Hydrol. Earth Syst. Sci.*, **14**(7), 1247–1258.
- Caballero, Y., V. Jomelli, P. Chevallier, and P. Ribstein (2002), Hydrological characteristics of slope deposits in high tropical mountains (Cordillera Real, Bolivia), *Catena*, **47**(2), 101–116.
- Caballero, Y., P. Chevallier, R. Gallaire, and R. Pillco (2004), Flow modelling in a high mountain valley equipped with hydropower plants: Rio Zongo Valley, Cordillera Real, Bolivia, *Hydrol. Processes*, **18**(5), 939–957.
- Casassa, G., P. López, B. Pouyaud, and F. Escobar (2009), Detection of changes in glacial run-off in alpine basins: Examples from North America, the Alps, central Asia and the Andes, *Hydrol. Processes*, **23**(1), 31–41.
- Cauvy-Fraunié, S., P. Andino, R. Espinosa, R. Calvez, F. Anthelme, D. Jacobsen, and O. Dangles, (2013), Glacial flood pulse effects on benthic fauna in equatorial high-Andean streams, *Hydrol. Processes*, **28**(6), 3008–3017, doi:10.1002/hyp.9866.
- Chevallier, P., B. Pouyaud, W. Suarez, and T. Condom (2011), Climate change threats to environment in the tropical Andes: Glaciers and water resources, *Reg. Environ. Change*, **11**(1), 179–187.
- Christensen, J. H., et al. (2007), Regional Climate Projections, in *Climate Change 2007: The Physical Science Basis, Contribution of Working Group I to the Fourth Assessment Report of the Intergovernmental Panel on Climate Change*, edited by S. Solomon et al., pp. 847–940, Cambridge Univ. Press, Cambridge, U. K.
- Clarke, G. K., F. Anslow, A. Jarosch, V. Radic, B. Menounos, T. Bolch, and E. Berthier (2013), Ice volume and subglacial topography for western Canadian glaciers from mass balance fields, thinning rates, and a bed stress model, *J. Clim.*, **26**(12), 4282–4303.
- Clarke, G. K., A.H. Jarosch, F. S. Anslow, V. Radic, and B. Menounos (2015), Projected deglaciation of western Canada in the twenty-first century, *Nat. Geosci.*, **8**, 372–377, doi:10.1038/ngeo2407.
- Condom, T., M. Escobar, D. Purkey, J. C. Pouget, W. Suarez, C. Ramos, J. Apaestegui, A. Tacsí, and J. Gomez (2012), Simulating the implications of glaciers' retreat for water management: A case study in the Rio Santa basin, Peru, *Water Int.*, **37**(4), 442–459.
- Cristea, N. C., J. D. Lundquist, S. P. Loheide, C. S. Lowry, and C. E. Moore (2013), Modeling how vegetation cover affects climate change impacts on streamflow timing and magnitude in the snowmelt-dominated upper Tuolumne Basin, Sierra Nevada, *Hydrol. Processes*, **28**(12), 3896–3918, doi:10.1002/hyp.9909.
- Cuffey, K. M., and W. S. B. Paterson (2010), *The Physics of Glaciers*, 4th ed., Butterworth-Heinemann, Oxford, U. K.
- Cuo, L., T. W. Giambelluca, A. D. Ziegler, and M. Nullet (2006), Use of the distributed hydrology soil vegetation model to study road effects on hydrological processes in Pang Khum Experimental Watershed, northern Thailand, *For. Ecol. Manage.*, **224**(1), 81–94.
- Elsner, M. M., L. Cuo, N. Voisin, J.S. Deems, A.F. Hamlet, J.A. Vano, and D. P. Lettenmaier, (2010), Implications of 21st century climate change for the hydrology of Washington State, *Clim. Change*, **102**(1–2), 225–260.
- Faticchi, S., V. Y. Ivanov, and E. Caporali (2011), Simulation of future climate scenarios with a weather generator, *Adv. Water Resour.*, **34**(4), 448–467.
- Faticchi, S., V. Y. Ivanov, and E. Caporali (2013), Assessment of a stochastic downscaling methodology in generating an ensemble of hourly future climate time series, *Clim. Dyn.*, **40**(7–8), 1841–1861.
- Favier, V., M. Falvey, A. Rabatel, E. Praderio, and D. López (2009), Interpreting discrepancies between discharge and precipitation in high-altitude area of Chile's Norte Chico region (26–32°S), *Water Resour. Res.*, **45**, W02424, doi:10.1029/2008WR006802.
- Fountain, A. G., and W. V. Tangborn (1985), The effect of glaciers on streamflow variations, *Water Resour. Res.*, **21**, 579–586.
- Franco, B., P. Ribstein, R. Saravia, and E. Tiriou (1995), Monthly balance and water discharge of an inter-tropical glacier: Zongo Glacier, Cordillera Real, Bolivia, *16 S. J. Glaciol.*, **41**(137), 61–67.
- Franco, B., M. Vuille, P. Wagnon, J. Mendoza, and J. E. Sicart (2003), Tropical climate change recorded by a glacier in the central Andes during the last decades of the twentieth century: Chacaltaya, Bolivia, *16 S. J. Geophys. Res.*, **108**(D5), 4154, doi:10.1029/2002JD002959.
- Gardner, A. S., et al. (2013), A reconciled estimate of glacier contributions to sea level rise: 2003 to 2009, *Science*, **340**, 6134, 852–857.
- Garreaud, R. D., M. Vuille, R. Compagnucci, and J. Marengo (2009), Present-day south american climate, *Palaeogeogr. Palaeoclimatol. Palaeoecol.*, **281**(3), 180–195.
- Gascoin, S., C. Kinnard, R. Ponce, S. Macdonell, S. Lhermitte, and A. Rabatel (2011), Glacier contribution to streamflow in two headwaters of the Huasco River, Dry Andes of Chile, *Cryosphere*, **5**(5), 1099–1113.
- Glen, J. W. (1955), The creep of polycrystalline ice, *Proc. R. Soc. London, Ser. A*, **228**, 519–538.

- Helgason, W., and Pomeroy, J. (2012), Problems closing the energy balance over a homogeneous snow cover during midwinter, *J. Hydrometeorol.*, *13*(2), 557–572.
- Huss, M., and D. Farinotti (2012), Distributed ice thickness and volume of all glaciers around the globe, *J. Geophys. Res.*, *117*, F04010, doi:10.1029/2012JF002523.
- Huss, M., D. Farinotti, A. Bauder, and M. Funk (2008), Modelling runoff from highly glacierized alpine drainage basins in a changing climate, *Hydrol. Processes*, *22*(19), 3888–3902.
- Huss, M., M. Zemp, P. C. Joerg, and N. Salzmann (2014), High uncertainty in 21st century runoff projections from glacierized basins, *J. Hydrol.*, *510*(2014), 35–48.
- Immerzeel, W. W., L. P. H., Van Beek, M. Konz, A. B. Shrestha, and M. F. P. Bierkens (2012), Hydrological response to climate change in a glacierized catchment in the Himalayas, *Clim. Change*, *110*(3–4), 721–736.
- Immerzeel, W. W., F. Pellicciotti, and M. F. P. Bierkens (2013), Rising river flows throughout the twenty-first century in two Himalayan glacierized watersheds, *Nat. Geosci.*, *6*(9), 742–745.
- IPCC (2014), Climate Change 2014: Impacts, adaptation, and vulnerability, in *Part A: Global and Sectoral Aspects, Contribution of Working Group II to the Fifth Assessment Report of the Intergovernmental Panel on Climate Change*, edited by C. B. Field et al., 1132 pp., Cambridge Univ. Press, Cambridge, U. K.
- Ivanov, V. Y., R. L. Bras, and D. C. Curtis (2007), A weather generator for hydrological, ecological, and agricultural applications, *Water Resour. Res.*, *43*, W10406, doi:10.1029/2006WR005364.
- Juen, I., G. Kaser, and C. Georges (2007), Modelling observed and future runoff from a glacierized tropical catchment (Cordillera Blanca, Perú), *Global Planet. Change*, *59*(1), 37–48.
- Kaser, G., J. G. Cogley, M. B. Dyurgerov, M. F. Meier, and A. Ohmura (2006), Mass balance of glaciers and ice caps: Consensus estimates for 1961–2004, *Geophys. Res. Lett.*, *33*, L19501, doi:10.1029/2006GL027511.
- La Freniere, J., and B. G. Mark (2014), A review of methods for estimating the contribution of glacial meltwater to total watershed discharge, *Prog. Phys. Geogr.*, *38*(2), 173–200.
- Lambrecht, A., and C. Mayer (2009), Temporal variability of the non-steady contribution from glaciers to water discharge in western Austria, *J. Hydrol.*, *376*, 353–361.
- Laramie, R. L., and J. C. Schaake Jr. (1972), Simulation of the continuous snowmelt process, *Parsons Lab. Tech. Rep. 143*, Mass. Inst. of Technol., Cambridge.
- Lejeune, Y., L. Bouilloud, P. Etchevers, P. Wagnon, P. Chevallier, J. E. Sicart, J. E. Martin, and F. Habets (2007), Melting of snow cover in a tropical mountain environment in Bolivia: Processes and modeling, *J. Hydrometeorol.*, *8*(4), 922–937.
- Luce, C. H., J. T. Abatzoglou, and Z. A. Holden (2013), The Missing Mountain Water: Slower westerlies decrease orographic enhancement in the Pacific Northwest USA, *Science*, *342*(6164), 1360–1364.
- Lundquist, J. D., N. E. Wayand, A. Massmann, M. P. Clark, F. Lott, and N. C. Cristea (2015), Diagnosis of insidious data disasters, *Water Resour. Res.*, *51*, 3815–3827, doi:10.1002/2014WR016585.
- Mahaffy, M. W. (1976), A three-dimensional numerical model of ice sheets: Tests on the Barnes Ice Cap, Northwest Territories, *J. Geophys. Res.*, *81*, 1059–1066.
- Mark, B. G., and G. O. Seltzer (2003), Tropical glacier meltwater contribution to stream discharge: A case study in the Cordillera Blanca, Peru, *J. Glaciol.*, *49*(165), 271–281.
- Minvielle, M., R. D. Garreaud (2011), Projecting rainfall changes over the South American Altiplano, *J. Clim.*, *24*, 4577–4583, doi:10.1175/JCLI-D-11-00051.1.
- Moore, R. D., S. W. Fleming, B. Menounos, R. Wheate, A. Fountain, K. Stahl, K. Holm, and M. Jakob (2009), Glacier change in western North America: Influences on hydrology, geomorphic hazards and water quality, *Hydrol. Processes*, *23*, 1 42–61.
- Moriasi, D. N., J. G. Arnold, M. W. Van Liew, R. L. Bingner, R. D. Harmel, and T. L. Veith (2007), Model evaluation guidelines for systematic quantification of accuracy in watershed simulations, *Trans. ASABE*, *50*(3), 885–900.
- Naz, B. S., C. D. Frans, G. K. C. Clarke, P. Burns, and D. P. Lettenmaier (2014), Modeling the effect of glacier recession on streamflow response using a coupled glacio-hydrological model, *Hydrol. Earth Syst. Sci.*, *18*, 787–802, doi:10.5194/hess-18-787-2014.
- Pellicciotti, F., M. Carenzo, R. Bordoy, and M. Stoffel (2014), Changes in glaciers in the Swiss Alps and impact on basin hydrology: Current state of the art and future research, *Sci. Total Environ.*, *493*, 1152–1170.
- Plummer, M. A., and F. M. Phillips (2003), A 2-D numerical model of snow/ice energy balance and ice flow for paleoclimatic interpretation of glacial geomorphic features, *Quat. Sci. Rev.*, *22*(14), 1389–1406.
- Pouyaud, B., M. Zapata, J. Yerren, J. Gomez, G. Rosas, W. Suarez, and P. Ribstein (2005), On the future of the water resources from glacier melting in the Cordillera Blanca, Peru, *Hydrol. Sci. J.*, *50*(6), 999–1022.
- Rabatel, A., A. Bermejo, E. Loarte, A. Soruco, J. Gomez, G. Leonardini, and J. E. Sicart (2012), Can the snowline be used as an indicator of the equilibrium line and mass balance for glaciers in the outer tropics?, *J. Glaciol.*, *58*(212), 1027–1036.
- Rabatel, A., et al. (2013), Current state of glaciers in the tropical Andes: A multi-century perspective on glacier evolution and climate change, *Cryosphere*, *7*, 81–102, doi:10.5194/tc-7-81-2013.
- Racoviteanu, A. E., Arnaud, Y., Williams, M. W., and Ordonez, J. (2008), Decadal changes in glacier parameters in the Cordillera Blanca, Peru, derived from remote sensing, *J. Glaciol.*, *54*(186), 499–510.
- Radić, V., and R. Hock (2011), Regionally differentiated contribution of mountain glaciers and ice caps to future sea-level rise, *Nat. Geosci.*, *4*(2), 91–94.
- Radić, V., R. Hock, and J. Oerlemans (2007), Volume-area scaling vs flowline modelling in glacier volume projections, *Ann. Glaciol.*, *46*, 234–240.
- Ragetti, S., and F. Pellicciotti (2012), Calibration of a physically based, spatially distributed hydrological model in a glacierized basin: On the use of knowledge from glaciometeorological processes to constrain model parameters, *Water Resour. Res.*, *48*, W03509, doi:10.1029/2011WR010559.
- Réveillet, M., A. Rabatel, F. Gillet-Chaulet, and A. Soruco (2015), Simulations of changes to Glacier Zongo, Bolivia (16 S), over the 21st century using a 3-D full-Stokes model and CMIP5 climate projections, *Ann. Glaciol.*, *56*(70), 89 pp.
- Ribstein, P., E. Tiriau, B. Francou, and R. Saravia (1995), Tropical climate and glacier hydrology: A case study in Bolivia, *J. Hydrol.*, *165*(1), 221–234.
- Sicart, J. E., P. Wagnon, and P. Ribstein (2005), Atmospheric controls of the heat balance of Zongo Glacier (16 S, Bolivia), *J. Geophys. Res.*, *110*, D12106, doi:10.1029/2004JD005732.
- Sicart, J. E., R. Hock, P. Ribstein, and J. P. Chazarin (2010), Sky long-wave radiation on tropical Andean glaciers: Parameterization and sensitivity to atmospheric variables, *J. Glaciol.*, *56*(199), 854–860, doi:10.3189/002214310794457182.

- Sicart, J. E., R. Hock, P. Ribstein, M. Litt, and E. Ramirez (2011), Analysis of seasonal variations in mass balance and meltwater discharge of the tropical Zongo Glacier by application of a distributed energy balance model, *J. Geophys. Res.*, *116*, D13105, doi:10.1029/2010JD015105.
- Soruco, A., C. Vincent, B. Francou, P. Ribstein, T. Berger, J. E. Sicart, and Y. Lejeune (2009), Mass balance of Glacier Zongo, Bolivia, between 1956 and 2006, using glaciological, hydrological and geodetic methods, *Ann. Glaciol.*, *50*(50), 1–8.
- Soruco, A., C. Vincent, A. Rabatel, B. Francou, E. Thibert, J. E. Sicart, and T. Condom (2015), Contribution of glacier runoff to water resources of La Paz city, Bolivia (16 S), *Ann. Glaciol.*, *56*(70), 147.
- Stahl, K., and R. D. Moore (2006), Influence of watershed glacier coverage on summer streamflow in British Columbia, Canada, *Water Resour. Res.*, *42*, W06201, doi:10.1029/2006WR005022.
- Stahl, K., R. D. Moore, J. M. Shea, D. Hutchinson, and A. J. Cannon (2008), Coupled modelling of glacier and streamflow response to future climate scenarios, *Water Resour. Res.*, *44*, W02422, doi:10.1029/2007WR005956.
- Storck, P., L. Bowling, P. Wetherbee, and D. P. Lettenmaier (1998), Application of a GIS based distributed hydrology model for prediction of forest harvest effects on peak stream flow in the Pacific Northwest, *Hydrol. Processes*, *12*(6), 889–904.
- Suarez, W., P. Chevallier, B. Pouyaud, and P. Lopez (2008), Modelling the water balance in the glacierized Parón Lake basin (White Cordillera, Peru), *Hydrol. Sci. J.*, *53*(1), 266–277.
- Tebaldi, C., R. L. Smith, D. Nychka, and L. Mearns (2005), Quantifying uncertainty in projections of regional climate change: A Bayesian approach to the analysis of multimodel ensembles, *J. Clim.*, *18*(10), 1524–1540.
- Uhlmann, B., F. Jordan, and M. Beniston (2012a), Modelling runoff in a Swiss glacierized catchment—Part I: Methodology and application in the Findelen basin under a long-lasting stable climate, *Int. J. Climatol.*, *33*(5), 1293–1300.
- Uhlmann, B., F. Jordan, and M. Beniston (2012b), Modelling runoff in a Swiss glacierized catchment—Part II: Daily discharge and glacier evolution in the Findelen basin in a progressively warmer climate, *Int. J. Climatol.*, *33*(5), 1301–1307.
- Urrutia, R., and M. Vuille (2009), Climate Change projections for the tropical Andes using a regional climate model: Temperature and precipitation simulations for the end of the 21st century, *J. Geophys. Res.*, *114*, D02108, doi:10.1029/2008JD011021.
- Vergara, W., A. Deeb, A. Valencia, R. Bradley, B. Francou, A. Zarzar, A. Grünwaldt, and Se. Haeussling (2007), Economic impacts of rapid glacier retreat in the Andes, *Eos Trans. AGU*, *88*(25), 261–264.
- Vuille, M., R. S. Bradley, and F. Keimig (2000), Interannual climate variability in the Central Andes and its relation to tropical Pacific and Atlantic forcing, *J. Geophys. Res.*, *105*, 12,447–12,460.
- Vuille, M., B. Francou, P. Wagnon, I. Juen, G. Kaser, B. G. Mark, and R. S. Bradley (2008), Climate change and tropical Andean glaciers: Past, present and future, *Earth Sci. Rev.*, *89*(3), 79–96.
- Wagnon, P., P. Ribstein, G. Kaser, and P. Berton (1999), Energy balance and runoff seasonality of a Bolivian glacier, *Global Planet. Change*, *22*(1), 49–58.
- Westrick, K. (1999), Soil depth calculation “aml.” [Available at www.hydro.washington.edu/Lettenmaier/Models/DHSVM/index.shtml, last accessed Feb. 2014.]
- Wigmosta, M. S., L. W. Vail, and D. P. Lettenmaier (1994), A distributed hydrology-vegetation model for complex terrain, *Water Resour. Res.*, *30*, 1665–1679.
- Yapo, P. O., H. V. Gupta, and S. Sorooshian, Multi-objective global optimization for hydrologic models, *J. Hydrol.*, *204*, 83–97, 1998.
- Zhao, Q., Z. Liu, B. Ye, Y. Qin, Z. Wei, and S. Fang (2009), A snowmelt runoff forecasting model coupling WRF and DHSVM, *Hydrol. Earth Syst. Sci.*, *13*(10), 1897–1906.